Inorganic Chemistry

Article

pubs.acs.org/IC

New Uses for Old Drugs: Attempts to Convert Quinolone Antibacterials into Potential Anticancer Agents Containing Ruthenium

Jakob Kljun,[†,‡] Ioannis Bratsos,[§,∥] Enzo Alessio,[§] George Psomas,[⊥] Urška Repnik,[⊗] Miha Butinar,[⊗] Boris Turk,[†,⊗,#] and Iztok Turel*[,†,‡]

[†]Faculty of Chemistry and Chemical Technology, University of Ljubljana, Aškerčeva 5, *SI*-1000 Ljubljana, Slovenia

[‡]EN→FIST Centre of Excellence, Dunajska 156, *SI*-1000 Ljubljana, Slovenia

[§]Dipartimento di Scienze Chimiche e Farmaceutiche, Università di Trieste, Via L. Giorgieri 1, *I*-34127 Trieste, Italy

[∥]Department of Physical Chemistry, NCSR "Demokritos", *GR*-15310 Ag. Paraskevi, Athens, Greece

[⊥]Department of General and Inorganic Chemistry, Faculty of Chemistry, Aristotle University of Thessaloniki, P.O. Box 123, *GR*-54124 Thessaloniki, Greece

[⊗]Jozef Stefan Institute, Jamova c. 39, *SI*-1000 Ljubljana, Slovenia

[#]CIPKEBIP Centre of Excellence, Jamova c. 39, *SI*-1000, Ljubljana

Supporting Information

ABSTRACT: Continuing the study of the physicochemical and biological properties of ruthenium-quinolone adducts, four novel complexes with the general formula [Ru([9]aneS$_3$)(dmso-κS)(quinolonato-κ^2O,O)](PF$_6$), containing the quinolones levofloxacin (**1**), nalidixic acid (**2**), oxolinic acid (**3**), and cinoxacin (**4**), were prepared and characterized in solid state as well as in solution. Contrary to their organoruthenium analogues, these complexes are generally relatively stable in aqueous solution as substitution of the dimethylsulfoxide (dmso) ligand is slow and not quantitative, and a minor release of the quinolonato ligand is observed only in the case of **4**. The complexes bind to serum proteins displaying relatively high binding constants. DNA binding was studied using UV−vis spectroscopy, cyclic voltammetry, and performing viscosity measurements of CT DNA solutions in the presence of complexes **1**−**4**. These experiments show that the ruthenium complexes interact with DNA via intercalation. Possible electrostatic interactions occur in the case of compound **4**, which also shows the most pronounced rate of hydrolysis. Compounds **2** and **4** also exhibit a weak inhibition of cathepsins B and S, which are involved in the progression of a number of diseases, including cancer. Furthermore, complex **2** displayed moderate cytotoxicity when tested on the HeLa cell line.

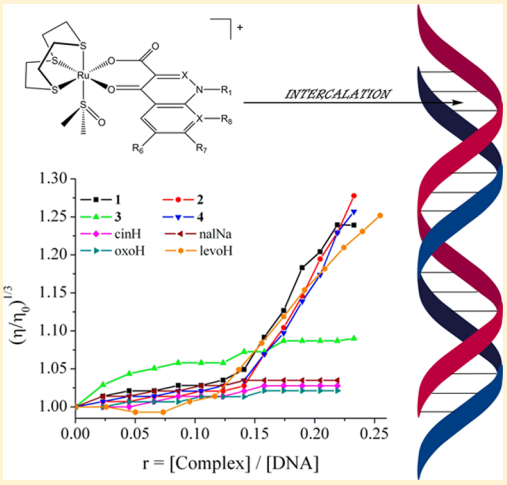

INTRODUCTION

Cisplatin is the first and by far the most widely used metal-based anticancer drug.[1] It is a pro-drug which is activated by hydrolysis of the two *cis*-bonded chlorido ligands that allows the binding of the *cis*-{Pt(NH$_3$)$_2$}$^{2+}$ fragment to nuclear DNA. This creates a kink in the DNA tertiary structure which prevents the replication of cancer cells. In the development of metal-based anticancer drugs platinum compounds still occupy the most important position. However, a number of coordination compounds of various other metals have also been evaluated.[2] Among them, the ruthenium complexes occupy the most prominent position as two compounds, namely, NAMI-A ([imH]*trans*-[RuCl$_4$(dmso-*S*)(im)], im = imidazole) and KP1019 ([indH]*trans*-[RuCl$_4$(ind)$_2$], ind = indazole), have been tested in clinical trials.[3,4] In the past decade the research has shifted mainly toward half-sandwich organoruthenium(II) complexes, and compounds bearing a wide variety of ligands were studied and evaluated for possible biological or medical applications.[5]

It has also been shown that the π-bonded aromatic ligands are not essential for the anticancer activity of ruthenium(II) complexes. The aromatic core can be substituted by another 6-electron face-capping ligand like the crown thioether 1,4,7-trithiacyclononane ([9]aneS$_3$), yet the complex still retains the properties that are needed to be suitable as a candidate for cancer treatment.[6,7]

Received: May 16, 2013

   dx.doi.org/10.1021/ic401220x | *Inorg. Chem.* XXXX, XXX, XXX−XXX

The exact mechanism of action of ruthenium compounds is not fully understood; however, recent research seems to favor the hypothesis that their interactions with proteins and enzymes specific for processes of cancer development and/or progress are crucial.[2] Most importantly, unlike the platinum(II) compounds, the different types of ruthenium compounds exhibit very different affinity and reactivity toward biomacromolecules and lower selectivity, since they readily interact and form adducts with various targets, including DNA (to a minor degree).[8−10] It is thus quite possible that ruthenium complexes hit multiple targets, and a combination of their action contributes to the observed beneficial properties. It is therefore important to investigate interactions with various potential targets to gain insight into the possible modes of action of these compounds and thus to be able to design novel and more effective drug candidates.

In this paper we present the continuation of our research on the physicochemical and biological properties of ruthenium-quinolone complexes. Quinolones are a family of synthetic antibacterial agents widely used in clinical practice. Nalidixic acid was the first quinolone introduced to clinical use in 1962 and since then more than 10,000 related compounds have been synthesized and tested as potential antibacterial agents, and more than thirty were, or still are, in clinical or veterinary use.[11] Besides their antibacterial activity, some quinolone derivatives with the extended aromatic ring system, namely, the quinobenzoxazines, were also shown to exhibit antitumor properties.[12]

Despite their widespread application, the exact mechanism of action of the quinolones is not fully understood. It is known that the quinolones bind to DNA, thus inhibiting the bacterial topoisomerase and preventing the replication of bacteria.[11] However, the binding mode of the quinolone to DNA is still uncertain. Various binding modes have been proposed[13] and the recent discovery of a topoisomerase-DNA-quinolone complex suggests that the role of metal ions is very important. In the aforementioned complex a magnesium ion binds the quinolone β-ketocarboxylate group and four water molecules, which in turn form hydrogen bonds with DNA nucleobases.[14]

Several metal complexes of compounds belonging to the quinolone family were reported in the past decades,[15] and their interactions with important biological macromolecules and their biological activity were investigated.[16,17] Our group recently reported the structures, hydrolytic and biological properties of organoruthenium complexes of quinolones that could potentially be used as anticancer agents.[9,18,19] The complex with the quinolone ofloxacin has shown binding to DNA which provoked a considerable shrinkage of the DNA tertiary structure and has proven to be moderately effective against the CH1 ovarian cancer cells. Moreover, the organoruthenium complex of the thionated derivative of the quinolone nalidixic acid showed considerable stability in aqueous solution and increased cytotoxicity toward various cancer cell lines and inhibition of cathepsins, enzymes involved in the development and progression of cancer and other diseases.[9,18,19]

Four novel ruthenium(II) complexes bearing the face-capping sulfur macrocycle [9]aneS$_3$, *S*-bonded dimethylsulfoxide (dmso-κS), and a quinolonato ligand (quinolonato-κ^2O,O) with the general formula [Ru([9]aneS$_3$)(dmso-κS)(quinolonato-κ^2O,O)](PF$_6$), where the quinolone ligand is levofloxacin (levo, **1**), nalidixic acid (nal, **2**), oxolinic acid (oxol, **3**), and cinoxacin (cin, **4**), respectively (Figure 1), were synthesized. The crystal structures of compounds **2** and **4** were

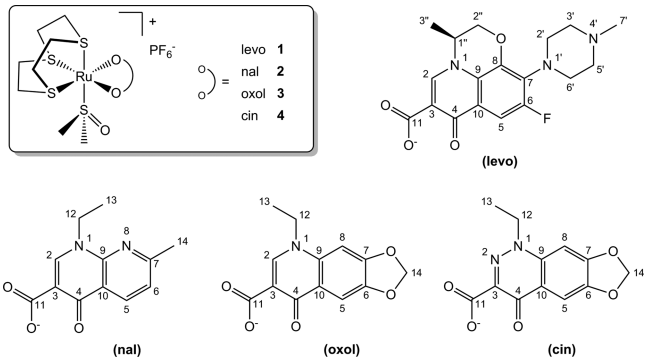

Figure 1. Schematic representation of the general formula of the new half sandwich [Ru([9]aneS$_3$)(dmso-κS)(quinolonato-κ^2O,O)](PF$_6$) compounds **1**−**4** and of the quinolonato ligands in anionic form used in the present work, with the numbering scheme used for the NMR characterization.

determined by X-ray diffraction analysis, and the stability of **1**−**4** in water solution was investigated by means of ^{1}H NMR spectroscopy. The interaction of complexes **1**−**4** with calf-thymus DNA (CT DNA) was studied, and a competitive study of the intercalative agent ethidium bromide (EB) was performed. The affinity of **1**−**4** toward bovine and human serum albumin (BSA and HSA) was investigated, and their binding constants were determined. The inhibitory potency of the compounds against cathepsins B and S, two enzymes of the cathepsin family, was also evaluated, as well as their cytotoxicity on two cancer cell lines (HeLa and A549).

1. EXPERIMENTAL PART

1.1. Materials and Instrumentation. All solvents, the quinolone ligands, CT DNA, BSA, HSA, EB, NaCl, tetraethylammonium perchlorate (TEAP), and trisodium citrate were purchased from Sigma-Aldrich. The ruthenium precursor [Ru([9]aneS$_3$)(dmso)$_3$](PF$_6$)$_2$ (**P1**) was prepared according to the reported procedure.[20] All the chemicals and solvents were reagent grade and were used as purchased.

Infrared spectra (ATR; Attenuated total reflectance) were recorded on a Perkin-Elmer Spectrum 100 spectrometer. The measurements were made in the range from 4000 to 600 cm^{-1}. Elemental analyses were performed on a Perkin-Elmer Elemental analyzer 2400 CHN. X-ray diffraction data were collected on a Nonius Kappa CCD diffractometer at 150 K for compound **2**·3H$_2$O and at room temperature for compound **4**·EtOH using graphite monochromated Mo-K_α radiation and processed using DENZO.[21] The structures were solved using SIR92.[22] A full-matrix least-squares refinement on *F* magnitudes with anisotropic displacement factors for all non-hydrogen atoms using SHELXL was employed.[23] The drawings, the analysis of bond lengths, angles, and intermolecular interactions was done using Mercury and Platon.[24] Hydrogen atoms were placed in geometrically calculated positions and were refined using a riding model.

Mono- (^{1}H (400 or 500 MHz), ^{13}C (101 or 126 MHz)) and bidimensional (^{1}H-^{1}H COSY, ^{1}H-^{13}C HSQC, ^{1}H-^{13}C HMBC) NMR spectra were recorded on a JEOL Eclipse 400FT or on a Varian 500 spectrometer (Trieste) or on a Bruker Avance III 500 spectrometer (Ljubljana). ^{1}H chemical shifts in D$_2$O were referenced to the internal standard 2,2-dimethyl-2,2-silapentane-5-sulfonate (DSS) at δ = 0.00, while in CD$_3$NO$_2$ were referenced to the peak of residual nondeuterated solvent (δ = 4.33); ^{13}C chemical shifts were referenced to the peak of residual nondeuterated nitromethane (δ = 62.8).

UV−visible (UV−vis) spectra were recorded in solution at concentrations in the range 10^{-5}−10^{-3} M on a Hitachi U-2001 dual beam spectrophotometer. Fluorescence spectra were recorded in solution on a Hitachi F-7000 fluorescence spectrophotometer. Viscosity experiments were carried out using an ALPHA L Fungilab

dx.doi.org/10.1021/ic401220x | *Inorg. Chem.* XXXX, XXX, XXX−XXX

rotational viscometer equipped with an 18 mL LCP spindle, and the measurements were performed at 100 rpm.

Cyclic voltammetry studies were performed on an Eco chemie Autolab Electrochemical analyzer. Cyclic voltammetry experiments were carried out in a 30 mL three-electrode electrolytic cell. The working electrode was platinum disk, a separate Pt single-sheet electrode was used as the counter electrode, and a Ag/AgCl electrode saturated with KCl was used as the reference electrode. The cyclic voltammograms of the complexes were recorded in 0.4 mM dimethylsulfoxide (DMSO) solutions and in 0.4 mM (1:2) DMSO:buffer solutions at v = 100 mV s^{-1} with TEAP and the buffer solution being the supporting electrolytes, respectively. Oxygen was removed by purging the solutions with pure nitrogen which had been previously saturated with solvent vapors. All electrochemical measurements were performed at 25.0 ± 0.2 °C.

1.2. Syntheses and Characterization. *General Synthetic Procedure for 1−4.* An 80.0 mg portion of the ruthenium precursor $[Ru([9]aneS_3)(dmso)_3](PF_6)_2$ (**P1**, 0.099 mmol) and 1 equiv of the appropriate quinolone (0.099 mmol) in acidic form with 5.0 mg of NaOMe (0.093 mmol), or just 1 equiv of nalidixic acid sodium salt hydrate in case of **2**, were suspended in 15 mL of MeOH. The suspension gradually dissolved as the reaction mixture was heated yielding a clear yellow solution, which was then refluxed for 2 h. The solvent was then rotary-evaporated, replaced by acetone, and $NaPF_6$ was removed by filtration. The solvent was again replaced by EtOH, and the formed product was collected by filtration, washed with EtOH and diethyl ether, and vacuum-dried.

*1.2.1. [Ru([9]aneS$_3$)(dmso-κS)(levo-κ^{2}O,O)](PF$_6$) (**1**).* This complex was prepared according to the general procedure using 35.9 mg of levofloxacin (0.099 mmol) affording 42.5 mg of **1** as yellow solid (Yield 49.5%). Crystals of complex **1** were obtained by slow evaporation of a methanol/ethanol solution.

Selected IR resonances (cm^{-1}, ATR): 3651, 2971, 1624, 1578, 1515, 1467, 1272, 1087, 830, 804. CHN: Calc. for $C_{26}H_{37}F_7N_3O_5PRuS_4 \cdot 1{,}5H_2O$ C, 35.01; H, 4.52; N, 4.71. Found C, 35.18; H, 4.37; N, 4.79.

NMR: ^{1}H NMR (400 MHz, D_2O) δ 8.98 (s, 1H, C^2H), 7.79 (d, J = 12.7 Hz, 1H, C^5H), 4.81 (overlapped with the peak of HOD, $C^{1''}H$), 4.60 (d, J = 11.8 Hz, 1H, $C^{2''}H_a$), 4.40 (m br, 1H, $C^{2''}H_b$), 3.51 (s br, 4H, $C^{2'}H_2/C^{6'}H_2$), 3.19 (s, 3H, CH_3 dmso), 3.15 (s, 3H, CH_3 dmso), 3.11−2.57 (m, 19H, $C^{3'}H_2/C^{5'}H_2$, CH_2 [9]aneS$_3$, $C^{7'}H_3$), 1.56 (t, J = 5.9 Hz, 3H, $C^{3''}H_3$).

The presence of two diasteromers is evident in the NMR spectra of **1** in CD_3NO_2, where almost all the resonances consist of two closely spaced peaks. The isolation and the full assignment of each isomer was not attempted.

^{1}H NMR (500 MHz, CD_3NO_2) δ 8.98 and 8.97 (2s, 2 × 1H, C^2H), 7.74 (d br, J = 12.9 Hz, 2 × 1H, C^5H), 4.77 (m br, 2 × 1H, $C^{1''}H$), 4.62 (d, J = 12.0 Hz, 2 × 1H, $C^{2''}H_a$), 4.45 and 4.43 (2d, J = 10.0 Hz, 2 × 1H, $C^{2''}H_b$), 3.57 (m br, 2 × 4H, $C^{2'}H_2/C^{6'}H_2$), 3.10 and 3.09 (2s, 2 × 3H, CH_3 dmso), 3.08−3.03 (m, 2 × 4H, $C^{3'}H_2/C^{5'}H_2$), 3.02 and 3.01 (2s, 2 × 3H, CH_3 dmso), 2.99−2.54 (m, 2 × 12H, CH_2 [9]aneS$_3$), 2.70 (s br, 2 × 3H, $C^{7'}H_3$), 1.64 and 1.62 (2d, J = 6.8 Hz, 2 × 3H, $C^{3''}H_3$).

^{13}C NMR (126 MHz, CD_3NO_2) δ 178.4 (C^4═O), 167.3 (C^{11}═O), 158.8 and 156.9 (C^6H), 150.3 (C^2H), 141.7 (C^8), 132.4 and 132.4 (C^7), 125.0 (C^9), 124.0 and 124.0 (C^{10}), 113.9 and 113.8 (C^3), 105.5 and 105.3 (C^5H), 69.8 and 69.8 ($C^{2''}H_2$), 57.6 and 57.6 ($C^{1''}$H), 56.7 ($C^{3'}H_2/C^{5'}H_2$), 50.4 ($C^{2'}H_2/C^{6'}H_2$), 46.0 ($C^{7'}H_3$), 43.8 (CH_3 dmso-S), 43.6 (CH_3 dmso-S), 36.2 and 36.2 (CH_2 [9]aneS$_3$), 35.6 and 35.5 (CH_2 [9]aneS$_3$), 34.3 and 34.2 (CH_2 [9]aneS$_3$), 33.5 and 33.4 (CH_2 [9]aneS$_3$), 31.4 and 31.3 (CH_2 [9]aneS$_3$), 31.2 and 31.1 (CH_2 [9]aneS$_3$), 18.5 and 18.4 ($C^{3''}H_3$).

*1.2.2. [Ru([9]aneS$_3$)(dmso-κS)(nal-κ^{2}O,O)](PF$_6$)·3H$_2$O (**2**·3H$_2$O).* This complex was prepared according to the general procedure using 27.0 mg of nalidixic acid sodium salt hydrate (0.099 mmol) affording 62.4 mg of **2** as yellow solid (Yield 79.8%). Crystals of **2** suitable for X-ray analysis (yellow needles) were obtained by dissolving the complex in a EtOH/MeOH mixture (ca. 5 mL; 4:1) followed by slow evaporation.

Selected IR resonances (cm^{-1}, ATR): 2989, 1622, 1604, 1573, 1492, 1447, 1258, 1080, 835, 804. CHN: Calc. for $C_{20}H_{29}F_6N_2O_4PRuS_4 \cdot 3H_2O$ C, 30.42; H, 4.47; N, 3.55. Found C, 30.27; H, 4.71; N, 3.69.

NMR: ^{1}H NMR (400 MHz, D_2O) δ 9.22 (s, 1H, C^2H), 8.71 (d, J = 8.3 Hz, 1H, C^5H), 7.55 (d, J = 8.3 Hz, 1H, C^6H), 4.77−4.60 (m, 2H, $C^{12}H_2$), 3.19 (s, 3H, CH_3 dmso-S), 3.16 (s, 3H, CH_3 dmso-S), 3.14−2.54 (m, 12H, CH_2 [9]aneS$_3$), 2.74 (s, 3H, $C^{14}H_3$), 1.51 (t, J = 7.1 Hz, 3H, $C^{13}H_3$).

^{1}H NMR (500 MHz, CD_3NO_2) δ 9.24 (s, 1H, C^2H), 8.72 (d, J = 8.3 Hz, 1H, C^5H), 7.52 (d, J = 8.3 Hz, 1H, C^6H), 4.81−4.68 (m, 2H, $C^{12}H_2$), 3.10 (s, 3H, CH_3 dmso-S), 3.02 (s, 3H, CH_3 dmso-S), 3.09−2.53 (m, 12H, CH_2 [9]aneS$_3$), 2.75 (s, 3H, $C^{14}H_3$), 1.56 (t, J = 7.2 Hz, 3H, $C^{13}H_3$).

^{13}C NMR (101 MHz, CD_3NO_2) δ 180.2 (C^4═O), 167.0 (C^{11}═O), 166.5 (C^7), 153.9 (C^2H), 148.3 (C^9), 137.5 (C^5H), 124.0 (C^6H), 121.6 (C^{10}), 115.4 (C^3), 49.1 ($C^{12}H_2$), 43.8 (CH_3 dmso-S), 43.6 (CH_3 dmso-S), 36.3 (CH_2 [9]aneS$_3$), 35.4 (CH_2 [9]aneS$_3$), 34.3 (CH_2 [9]aneS$_3$), 33.4 (CH_2 [9]aneS$_3$), 31.4 (CH_2 [9]aneS$_3$), 31.0 (CH_2 [9]aneS$_3$), 25.5 ($C^{14}H_3$), 15.6 ($C^{13}H_3$).

*1.2.3. [Ru([9]aneS$_3$)(dmso-κS)(oxol-κ^{2}O,O)](PF$_6$) (**3**).* This complex was prepared according to the general procedure, slightly modified, using 25.9 mg of oxolinic acid (0.099 mmol). After refluxing in MeOH, the product started to precipitate as pale yellow solid upon cooling. The precipitation was completed after the concentration of the solution to about 4 mL affording 62.3 mg of **3** (Yield 82.8%).

Selected IR resonances (cm^{-1}, ATR): 3000, 1636, 1583, 1563, 1466, 1264, 1084, 1033, 1022, 831. CHN: Calc. for $C_{21}H_{28}F_6NO_6PRuS_4$ C, 32.98; H, 3.61; N, 1.83. Found C, 32.32; H, 3.98; N, 1.71.

NMR: ^{1}H NMR (400 MHz, D_2O) δ 8.95 (s, 1H, C^2H), 7.81 (s, 1H, C^5H), 7.39 (s, 1H, C^8H), 6.21 (s, 2H, $C^{14}H_2$), 4.49 (dd, J = 14.7, 7.7 Hz, 2H, $C^{12}H_2$), 3.18 (s, 3H, CH_3 dmso), 3.15 (s, 3H, CH_3 dmso), 3.13−2.54 (m, 12H, CH_2 [9]aneS$_3$), 1.51 (t, J = 7.1 Hz, 3H, $C^{13}H_3$).

^{1}H NMR (500 MHz, CD_3NO_2) δ 8.98 (s, 1H, C^2H), 7.81 (s, 1H, C^5H), 7.31 (s, 1H, C^8H), 6.22 (s, 2H, $C^{14}H_2$), 4.52 (q, J = 7.2 Hz, 2H, $C^{12}H_2$), 3.09 (s, 3H, CH_3 dmso), 3.02 (s, 3H, CH_3 dmso), 3.08−2.52 (m, 12H, CH_2 [9]aneS$_3$), 1.58 (t, J = 7.2 Hz, 3H, $C^{13}H_3$).

^{13}C NMR (126 MHz, CD_3NO_2) δ 177.8 (C^4═O), 167.4 (C^{11}═O), 155.1 (C^7), 151.5 (C^2H), 149.3 (C^6), 136.9 (C^9), 125.3 (C^{10}), 105.0 ($C^{14}H_2$), 104.2 (C^5H), 97.0 (C^8H), 52.0 ($C^{12}H_2$), 43.8 (CH_3 dmso-S), 43.5 (CH_3 dmso-S), 36.2 (CH_2 [9]aneS$_3$), 35.4 (CH_2 [9]aneS$_3$), 34.3 (CH_2 [9]aneS$_3$), 33.4 (CH_2 [9]aneS$_3$), 31.4 (CH_2 [9]aneS$_3$), 31.1 (CH_2 [9]aneS$_3$), 14.9 ($C^{13}H_3$).

*1.2.4. [Ru([9]aneS$_3$)(dmso-κS)(cin-κ^{2}O,O)](PF$_6$)·EtOH (**4**·EtOH).* This complex was prepared according to the general procedure using 26.0 mg of cinoxacin (0.099 mmol) affording 74.4 mg of **4** as a yellow-orange solid (Yield 92.9%). Crystals suitable for X-ray analysis were obtained from a MeOH/EtOH 1:1 solution upon slow evaporation at room temperature.

Selected IR resonances (cm^{-1}, ATR): 2981, 1618, 1601, 1519, 1468, 1272, 1089, 1034, 829, 784. CHN: Calc. for $C_{20}H_{27}F_6N_2O_6PRuS_4 \cdot C_2H_6O$ C, 29.96; H, 3.90; N, 3.50. Found C, 30.33; H, 3.87; N, 3.34.

NMR: ^{1}H NMR (500 MHz, D_2O) δ 7.74 (s, 1H, C^5H), 7.49 (s, 1H, C^8H), 6.29 (s, 2H, $C^{14}H_2$), 4.76 (overlapped with HOD, $C^{12}H_2$), 3.22 (s, 3H, CH_3 dmso-S), 3.19 (s, 3H, CH_3 dmso-S), 3.15−2.55 (m, 12H, CH_2 [9]aneS$_3$), 1.56 (t, J = 7.3 Hz, 3H, $C^{13}H_3$).

^{1}H NMR (500 MHz, CD_3NO_2) δ 7.74 (s, 1H, C^5H), 7.37 (s, 1H, C^8H), 6.29 (d, J = 2.1 Hz, 2H, $C^{14}H_2$), 4.75 (q, J = 7.3 Hz, 2H, $C^{12}H_2$), 3.14 (s, 3H, CH_3 dmso-S), 3.07 (s, 3H, CH_3 dmso-S), 3.11−3.04 (m, 1H, CH_2 [9]aneS$_3$), 3.02−2.69 (m, 9H, CH_2 [9]aneS$_3$), 2.67−2.60 (m, 1H, CH_2 [9]aneS$_3$), 2.60−2.53 (m, 1H, CH_2 [9]aneS$_3$), 1.59 (t, J = 7.3 Hz, 3H, $C^{13}H_3$).

^{13}C NMR (126 MHz, CD_3NO_2) δ 172.0 (C^4═O), 165.3 (C^{11}═O), 156.6 (C^7), 151.4 (C^6), 139.8 (C^9), 138.5 (C^3H), 127.0 (C^{10}), 105.6 ($C^{14}H_2$), 102.2 (C^5H), 95.9 (C^8H), 55.7 ($C^{12}H_2$), 43.7 (CH_3 dmso-S), 43.6 (CH_3 dmso-S), 36.2 (CH_2 [9]aneS$_3$), 35.6 (CH_2 [9]aneS$_3$), 34.2 (CH_2 [9]aneS$_3$), 33.5 (CH_2 [9]aneS$_3$), 31.3 (CH_2 [9]aneS$_3$), 31.2 (CH_2 [9]aneS$_3$), 14.2 ($C^{13}H_3$).

dx.doi.org/10.1021/ic401220x | *Inorg. Chem.* XXXX, XXX, XXX−XXX

1.3. Bioassays. To study the biological behavior (interactions with DNA, serum albumins, cathepsin inhibition, and cytotoxicity) of complexes **1**−**4**, they were initially dissolved in DMSO (1 mM), and the resultant solutions were used for no longer than 2 h. Mixing of such solutions with the aqueous solutions used in biological studies never exceeded 5% DMSO (v/v) in the final solution, which was needed because of low aqueous solubility of some of the complexes and ligands. Control experiments performed with 5% DMSO showed no influence on the final results.

1.3.1. DNA Binding Studies. DNA stock solution was prepared by dilution of CT DNA in the buffer (containing 15 mM trisodium citrate and 150 mM NaCl at pH 7.0) followed by exhaustive stirring for 3 days, and kept at 4.0 °C for no longer than a week. The stock solution of CT DNA gave a ratio of UV absorbance at 260 and 280 nm (A_{260}/A_{280}) of 1.89, indicating that the DNA was sufficiently free of protein contamination. The DNA concentration per nucleotide was determined by UV absorbance measurements at 260 nm after 1:20 dilution using ε = 6600 M^{-1} cm^{-1}.[17]

The interaction of the quinolones and complexes **1**−**4** with CT DNA has been studied with UV spectroscopy to investigate the possible binding modes and to calculate the binding constants (K_b). In UV titration experiments, the spectra of CT DNA in the presence of each compound have been recorded for a constant CT DNA concentration at diverse [compound]:[DNA] ratios (r). The DNA-binding constants of the compounds, K_b, have been determined according to Supporting Information, eq S1 using the UV spectra recorded for a constant concentration of the compounds in the absence or presence of CT DNA for diverse r values.[17] Control experiments with DMSO were performed, and no changes in the spectra of CT DNA were observed.

Interaction of complexes **1**−**4** with CT DNA has been also investigated by monitoring the changes observed in the cyclic voltammogram of a 0.40 mM 1:2 DMSO:buffer solution of complex upon addition of CT DNA at diverse r values. The buffer was also used as the supporting electrolyte, and the cyclic voltammograms were recorded at ν = 100 mV s^{-1}.

The viscosity of a DNA solution has been measured in the presence of increasing amounts of complexes **1**−**4**. The relation between the relative solution viscosity (η/η_0) and DNA length (L/L_0) is given by the equation $L/L_0 = (\eta/\eta_0)^{1/3}$, where L_0 denotes the apparent molecular length in the absence of the compound.[25] The obtained data are presented as $(\eta/\eta_0)^{1/3}$ versus r, where η is the viscosity of DNA in the presence of the compound, and η_0 is the viscosity of DNA alone in buffer solution.

The competitive studies of each compound with EB have been investigated with fluorescence spectroscopy to examine whether the compound can displace EB from its EB-DNA complex. The EB-DNA complex was prepared by adding 20 μM EB and 26 μM CT DNA in buffer (150 mM NaCl and 15 mM trisodium citrate at pH 7.0). The possible intercalating effect of the quinolones and complexes **1**−**4** with the DNA was studied by adding a certain amount of a solution of the compound step by step into the solution of the EB-DNA complex. The influence of the addition of each compound to the EB-DNA complex solution has been obtained by recording the variation of fluorescence emission spectra. The Stern−Volmer equation (Supporting Information, eq S2) is used to evaluate the quenching efficiency for each compound.[17]

1.3.2. Albumin Binding Studies. The protein binding study was performed by tryptophan fluorescence quenching experiments using bovine (BSA, 3 μM) or human serum albumin (HSA, 3 μM) in buffer (containing 15 mM trisodium citrate and 150 mM NaCl at pH 7.0). Quenching of the emission intensity of tryptophan residues of BSA at 342 nm or HSA at 351 nm was monitored using the quinolones and complexes **1**−**4** as quenchers with increasing concentration (up to 2.2 × 10^{-5} M).[17,26] Fluorescence spectra were recorded in the range 300−500 nm at an excitation wavelength of 296 nm. The fluorescence spectra of the compounds in buffer solutions were recorded under the same experimental conditions, and no fluorescence emission was recorded. The Stern−Volmer and Scatchard equations (Supporting Information, eqs S3−S5) and graphs have been used to study the interaction of the compounds with serum albumins and calculate the corresponding constants.[17]

1.3.3. Cytotoxicity Studies. Human cervix carcinoma (HeLa) and non small cell lung carcinoma (A549) cells used in the experiment were obtained from the ECACC (European Collection of Cell Cultures, Public Health England; HeLa) or DSMZ (Leibniz-Institute DSMZ-Deutche Sammlung von Mikroorganismen and Zellkulturen GmbH; A549) and maintained in MEM (Minum Essential Medium, PAA) supplemented with 10% fetal bovine serum (Sigma), 2 mM L-glutamine (Invitrogen), 100 units of penicillin, 100 μg/mL streptomycin (Invitrogen), and 1% nonessential amino acids (Invitrogen) at 37.0 °C in a humidified 5% CO_2 atmosphere. Cells were harvested by trypsinization and seeded in 96-well transparent plates (PTT) at a final volume of 100 μL and densities of 4 × 10^3 cells per well. Cytotoxicity was then determined by the colorimetric MTT assay (3-[4,5-Dimethylthiazol-2-yl]-2,5-diphenyltetrazolium bromide; Thiazolyl blue, Sigma Aldrich) in triplicate essentially as described previously.[9]

1.3.4. Cathepsin Inhibition Studies. Recombinant human cathepsins B and S were prepared as described earlier.[27] Initial solutions of the compounds were prepared in DMSO. Subsequent dilutions were made in 100 mM phosphate buffer, pH 6.0. Inhibition of cathepsins was then determined essentially as described previously.[9]

2. RESULTS AND DISCUSSION

2.1. Synthesis and Characterization of the Complexes. Reaction of [Ru([9]aneS$_3$)(dmso)$_3$](PF$_6$)$_2$ (**P1**) with one molar equivalent of the appropriate quinolone in refluxing methanol and in the presence of sodium methoxide led to the isolation of cationic compounds of the general formula [Ru([9]aneS$_3$)(dmso-κS)(*O*-*O*′)](PF$_6$), where *O*-*O*′ = levo (**1**), oxol (**3**), and cin (**4**). Compound **2** was prepared in a similar manner, but using the sodium salt of nalidixic acid (nal-Na) because of its commercial availability. Attempts to isolate the neutral coordination compounds with general formula [Ru([9]aneS$_3$)Cl(*O*-*O*′)], analogues of the previously described organometallic complexes [Ru(η^6-p-cym)Cl(*O*-*O*′)] (*O*-*O*′ = oflo, nal, cin),[18,19] by reacting the neutral precursor [Ru([9]aneS$_3$)Cl$_2$(dmso-κS)] with the appropriate quinolone ligand in the presence of a base were unsuccessful and often led to the isolation of mixtures of the dmso derivative [Ru([9]-aneS$_3$)(dmso-κS)(*O*-*O*′)](Cl) and of the aqua derivative [Ru([9]aneS$_3$)(OH$_2$)(*O*-*O*′)](Cl), as proven by NMR experiments. All new complexes were characterized by elemental analysis and IR spectroscopy in solid state and by NMR spectroscopy in solution state. The solid state structures of **2** and **4** were also determined by X-ray crystallography (Supporting Information, Table S1).

Crystals of compound **1** were obtained, and the structure was partially solved which confirmed the proposed structure. However, they could not be adequately refined because of the low crystal quality, the presence of various disordered solvate molecules, and the presence of rotational disorder on the anionic species. On the other hand, the structures of complexes **2** and **4** were unambiguously refined. In all analyzed complex cations, the Ru center displays the expected slightly distorted octahedral geometry, and the coordination sphere is composed of the tridentate [9]aneS$_3$ ligand in facial geometry, of one quinolonato ligand acting as chelating ligand through the pyridone, and the carboxylato oxygen atoms and of one dmso molecule bonded through sulfur (Figure 2 and 3).

The Ru−S bond length values in complexes **2** and **4** are comparable to those in the previously published crystal structures of [Ru([9]aneS$_3$)(dmso-κS)(*O*,*O*′-ligand)] complexes bearing dianionic dicarboxylate ligands (oxalate,

dx.doi.org/10.1021/ic401220x | Inorg. Chem. XXXX, XXX, XXX−XXX

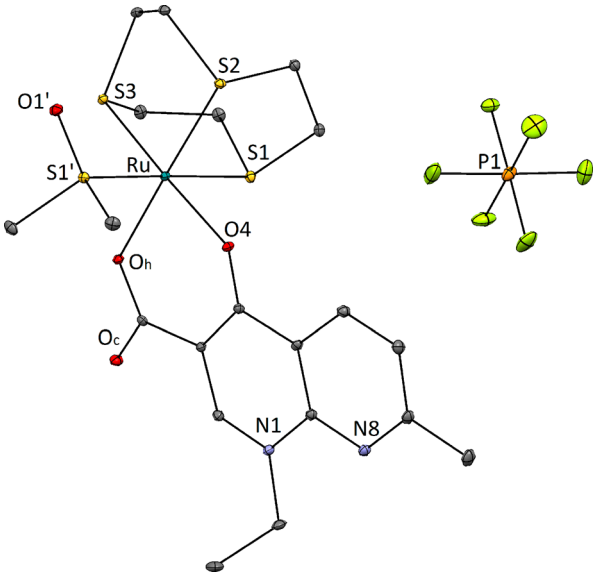

Figure 2. Crystal structure of compound [Ru([9]aneS$_3$)(dmso-κS)(nal)](PF$_6$)·3H$_2$O (**2**·3H$_2$O) with heteroatom labeling. The hydrogen atoms and water molecules are omitted for clarity. The thermal ellipsoids are shown at 20% probability level. Selected bond lengths: Ru–S1′ = 2.256(2) Å, Ru–S1 = 2.351(2) Å, Ru–S2 = 2.294(2) Å, Ru–S3 = 2.289(2) Å, Ru–O4 = 2.088(2) Å, Ru–O$_h$ = 2.104(2) Å.

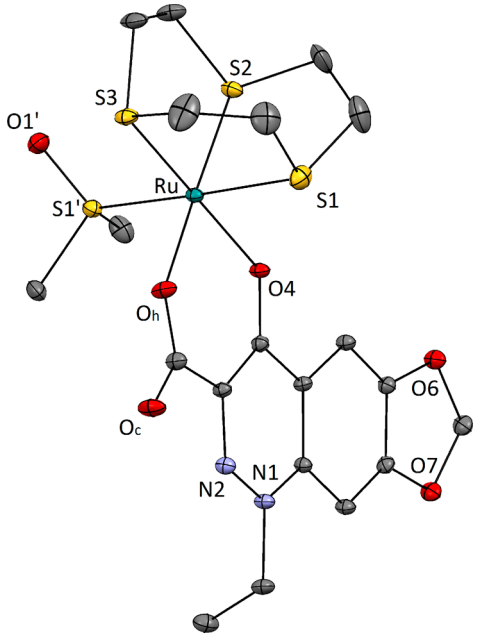

Figure 3. Crystal structure of compound [Ru([9]aneS$_3$)(dmso-κS)(cin)](PF$_6$)·EtOH (**4**·EtOH) with heteroatom labeling. The hydrogen atoms, the EtOH, and the hexafluorophosphate anion are omitted for clarity. The thermal ellipsoids are shown at 20% probability level. Selected bond lengths: Ru–S1′ = 2.269(3) Å, Ru–S1 = 2.345(3) Å, Ru–S2 = 2.284(3) Å, Ru–S3 = 2.281(3) Å, Ru–O4 = 2.097(2) Å, Ru–O$_h$ = 2.085(3) Å.

malonate) which are structurally the most similar complexes with known crystal structure so far, even though they have a different charge.[7]

In comparison to the organoruthenium complexes with quinolones previously described by our group, the Ru–O bond lengths in the case of the pyridone oxygen remain the same while in the case of the carboxylate oxygen a slight elongation is observed (Table 1)

As mentioned before, the quality of the crystals of compound **1** did not permit adequate refinement, yet it was evident from the presence of a different number of counterions, that upon standing in a saturated solution for few weeks compound **1** crystallized as a dicationic complex with the ligand levo in its zwitterionic form, with the protonated N4′ piperazine nitrogen atom.

Complex **4**·EtOH presents a fairly simple structure (Figure 3) devoid of supramolecular motifs, except for a hydrogen bond between the solvate ethanol molecule and the unbound carboxylate oxygen atom of the cinoxacinato ligand. On the other hand, in complex **2**·3H$_2$O, two of the cocrystallized water molecules (O51 and O52) are bound by hydrogen bonds which results in the formation of a helix about the screw axis. The cationic complex species of **2** is directly linked to the helix through a hydrogen bond to the ruthenium-bound carboxylate oxygen. The free carboxylic oxygen forms an additional hydrogen bond to the third water molecule (O50) which is then bound to the second helix-forming water molecule (Figure 4). The hydrogen bond lengths and angles are given in Supporting Information, Table S1b. The structure is further stabilized by weak hydrogen interactions between the O50 water molecule and the hexafluorophosphate anion.

The new complexes are soluble in H$_2$O, although they show a remarkable difference in their solubility: 10 mM aqueous solutions of complexes **1** and **4** can easily be prepared, while the solubility of complexes **2** and **3** is one- and two orders of magnitude lower, respectively. ^{1}H NMR studies were thus performed mainly in the biologically relevant D$_2$O solvent at about 1 mM except for **3**, for which a saturated solution was prepared by brief gentle heating and sonication followed by the filtration of the undissolved product. However, since these compounds hydrolyze in water (see below) it was not possible to record the ^{13}C NMR spectra of the intact species in D$_2$O. Therefore, proton and, in particular, carbon NMR spectra were recorded also in CD$_3$NO$_2$, where complexes are stable and well soluble. The full assignment of the proton and carbon NMR spectra of all complexes was performed by combination of 1D (^{1}H and ^{13}C) and 2D (^{1}H-^{1}H COSY, phase sensitive ^{1}H-^{13}C HSQC and ^{1}H-^{13}C HMBC) NMR experiments in either D$_2$O or CD$_3$NO$_2$ (see Supporting Information, Figures S1–S13).

All products share a common structural feature: the tridentate thioether macrocycle 1,4,7-trithiacyclononane ([9]-aneS$_3$) coordinated to the metal center in a facial manner. The methylene protons of this face-capping ligand provide a characteristic pattern of resonances in the ^{1}H NMR spectrum, a manifold of partially overlapping multiplets in the region 3.20–2.50 ppm. This pattern, with minor differences, is observed in the NMR spectra of all the studied complexes and will not be discussed further. In addition, as the *O-O′* ligands are not symmetrical, in all complexes the two methyl groups of the dmso are diastereotopic and resonate as two singlets in the region typical for *S*-bound dmso.

The ^{1}H NMR spectrum of **1** in D$_2$O displays two aromatic resonances: one singlet (δ = 8.98) attributed to the C^{2}H (see Figure 1 in the Introduction section for atom numbering) and one doublet (δ = 7.79), because of the coupling with the adjacent F, assigned to the C^{5}H. The diastereotopic protons of C$^{2''}$H$_2$ resonate as one doublet and one broad multiplet (δ = 4.60 and 4.40, respectively) that are coupled to each other in the ^{1}H-^{1}H COSY spectrum (Supporting Information, Figure

dx.doi.org/10.1021/ic401220x | *Inorg. Chem.* XXXX, XXX, XXX–XXX

Table 1. Selected Bond Distances (Å) and Angles (deg) in Ruthenium-Quinolone Complexes

	Ru−O4	Ru−O_h	O4−Ru−O_h
[(η^6-cymene)Ru(nal)Cl][19]	2.087(2)	2.070(2)	87.30(8)
[(η^6-cymene)Ru(cin)Cl][19]	2.099(2)	2.071(2)	84.94(8)
[(η^6-cymene)Ru(oflo)Cl][18]	2.071(2)	2.069(2)	85.30(7)
[Ru([9]aneS$_3$)(dmso-κS)(nal)](PF$_6$), **2**	2.088(2)	2.104(2)	88.92(7)
[Ru([9]aneS$_3$)(dmso-κS)(cin)](PF$_6$), **4**	2.097(2)	2.085(3)	87.02(11)

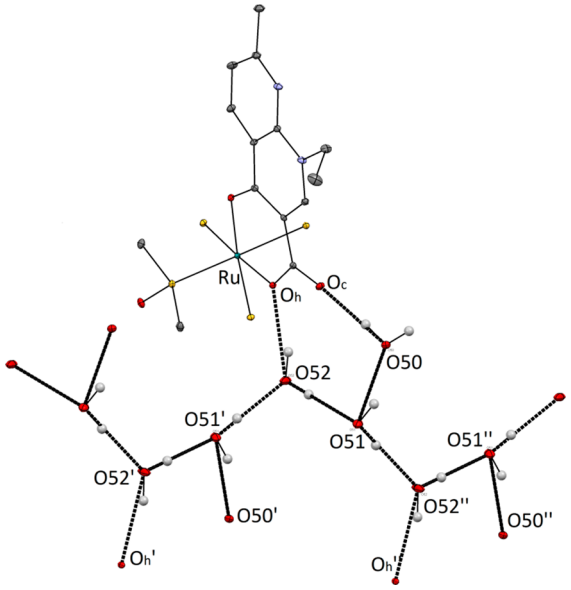

Figure 4. Hydrogen bonds in the crystal structure of compound **2**·3H_2O with heteroatom. Non relevant hydrogen atoms and the carbon atoms of the ligand [9]aneS$_3$ are omitted for clarity. The thermal ellipsoids are shown at 20% probability level.

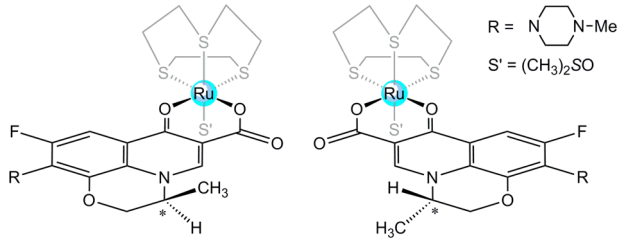

Figure 5. Perspective view of the two diastereomers formed by the chiral chelating ligand levo on the Ru center. The chiral center on the levo ligand is indicated with (*).

S9) and to the same carbon resonance in the ^{1}H-^{13}C HSQC spectrum (Supporting Information, Figure S10), while the C$^{1''}$H is overlapped with the intense resonance of the HOD. In the upfield region, besides the dmso (singlets at δ = 3.19 and 3.15 ppm) and the [9]aneS$_3$ peaks the spectrum displays also a broad singlet (δ = 3.51, 4H) attributed to the C$^{2'}$H$_2$ and C$^{6'}$H$_2$ of the piperazine ring and a broad triplet assigned to the methyl C$^{3''}$H$_3$; the peaks of C$^{3'}$H$_2$ and C$^{5'}$H$_2$ of the piperazine and the methyl C$^{7'}$H$_3$ are partially overlapped with the multiplets of [9]aneS$_3$ and were identified by the phase sensitive ^{1}H-^{13}C HSQC spectrum (Supporting Information, Figure S10). Worth noting, all resonances of levo are downfield shifted compared to the free ligand and in particular those of C^{2}H and C^{5}H (δ = 8.35 and 7.54, respectively, in free levo), which is indicative for the binding of levo on the Ru center.

Binding of the chiral ligand levo (i.e., (*S*)-enantiomer) on the Ru center is expected to produce two equally abundant diastereomers (Figure 5), since Ru also becomes chiral. The formation of both isomers was not obvious from the NMR experiments in D_2O, where only one set of resonances was observed. Conversely, the presence of both isomers is evident when NMR spectroscopy was carried out in CD_3NO_2. In the ^{1}H NMR spectrum of **1** in CD_3NO_2, although the pattern is similar to that found in D_2O, almost all peaks are split in two equally intense sets, each attributed to one of the two diastereomers; this splitting is predominantly evident for the singlets of the methyl groups of the dmso ligand (Supporting Information, Figure S1). The presence of both diasteromers is more obvious in the ^{13}C NMR spectrum of **1**, where again almost all the resonances are split into two closely spaced singlets (Supporting Information, Figure S2). For example, the methylene carbons of the [9]aneS$_3$ ligand resonate as 12 well resolved peaks.

The ^{1}H NMR spectrum of **2** in D_2O or in CD_3NO_2 (Supporting Information, Figure S3) is consistent with the molecular structure found in solid state. The nal ligand displays the expected pattern of resonances: one singlet and two doublets in the aromatic region attributed respectively to the C^{2}H, C^{5}H, and C^{6}H, one multiplet (δ = 4.70 in D_2O and 4.74 in CD_3NO_2) assigned to the C^{12}H$_2$, and two intense resonances, one singlet and one triplet, in the upfield region for the methyl groups C^{14}H$_3$ and C^{13}H$_3$, respectively. In D_2O, all resonances of the nal are shifted downfield compared to the free ligand because of its binding on the Ru center. For easier analysis and comparison of the ^{1}H and ^{13}C NMR spectra see Supporting Information, Tables S2 and S3.

The ^{13}C NMR spectrum of **2** in CD_3NO_2 (Supporting Information, Figure S4) is consistent also with the geometry and the low symmetry of the complex: six resonances for the unequivalent methylene carbons of the [9]aneS$_3$ ligand and two signals (very closely spaced) for the carbons of the diastereotopic methyl groups of the dmso ligand together with the expected peaks of the bound nal.

The oxol ligand is similar to nal with the differences that it bears a dioxolyl moiety at C^6 and C^7 and that the N^8 in nal is replaced by C^{8}H in oxol (see Figure 1). Accordingly, the ^{1}H spectrum of **3**, either in D_2O or in CD_3NO_2 (Supporting Information, Figure S5), is similar to that of **2** with few differences: the resonance of C^{5}H is now a singlet, while the doublet for C^{6}H and the singlet for the C^{14}H$_3$ in the spectrum of **2** have been replaced by two singlets, for C^{8}H and for C^{14}H$_3$ respectively, in the spectrum of **3**. The ^{13}C NMR spectrum of **3** in CD_3NO_2 (Supporting Information, Figure S6) is consistent also with the proposed geometry, and the low symmetry, of the complex.

Complex **4** bears the cin ligand, which is a quinolone very similar to oxol: only the C^{2}H of oxol is replaced by a nitrogen atom in cin. Owing to this similarity, the ^{1}H and ^{13}C NMR spectra of complex **4** in D_2O and in CD_3NO_2 are very similar to

dx.doi.org/10.1021/ic401220x | *Inorg. Chem.* XXXX, XXX, XXX−XXX

those of **3**, with the obvious absence of the C^2H resonance (Supporting Information, Figures S7 and S8).

Complexes **1**−**4** display similar IR spectra, with bands attributed to the asymmetric (1636−1618 cm^{-1}) and symmetric (1468−1447 cm^{-1}) stretching modes for the carboxyl groups and to the C═O (1578−1519 cm^{-1}) of the quinolone ligands, which are in agreement with the binding mode of the quinolones, that is, chelating through the oxygens of the carboxylate group and of the pyridone. In addition, the bands in the region 1089−1080 cm^{-1} and 835−829 cm^{-1} attributed to the S═O stretching of the *S*-bonded dmso and to the PF_6^- counterion, respectively, are clearly distinguishable.

The fluorescence emission spectra of the complexes have been recorded in DMSO solution. As an example, the fluorescence excitation and emission spectra for complexes **3** and **4** are shown in Supporting Information, Figure S14. The complexes exhibit an intense emission band with $\lambda_{em,max}$ lying in the region 444−495 nm when excited at $\lambda_{exc,max}$ 343−430 nm (Supporting Information, Table S4).

2.2. Chemical Behavior in Aqueous Solution. The chemical behavior of compounds **1**−**4** in aqueous solution was investigated by ^1H NMR spectroscopy at room temperature in view of their potential biological activity and interactions with biological macromolecules. The chemical changes in the spectra were monitored mainly through the aromatic resonances of the quinolone ligands and the dmso resonances, since the multiplets of [9]aneS_3 are unsuitable for monitoring purposes.

All new complexes exhibit very similar behavior in aqueous solution. They are relatively stable: no rapid changes were observed in their ^1H NMR spectra after dissolution in D_2O. Slow formation of the aqua species [Ru([9]aneS_3)(OH_2)(*O*-*O*′)]$^+$ (*O*-*O*′ = levo (**1a**), nal (**2a**), oxol (**3a**), and cin (**4a**); Figure 6) was indicated by the gradual decrease of the two

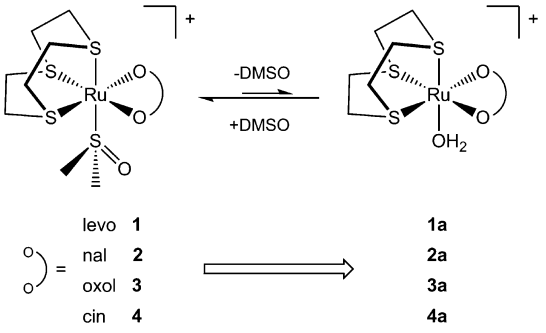

Figure 6. Chemical behavior of compounds **1**−**4** in aqueous solution.

dmso-S singlets and the corresponding growth of the free dmso resonance at δ = 2.71 ppm. After several hours the systems reached equilibria between the intact and aquated species. The time to reach equilibrium and the ratio between the intact and aqua species varies, depending mainly on the quinolone ligand. Complex **1** reaches equilibrium after about 24 h with a 7:3 ratio between **1** and **1a**, according to the integration of the aromatic resonances (Supporting Information, Figure S11). The same ratio was detected between **2** and **2a**, but equilibrium was reached after about 2 days (Figure 7). The aquation of **3** is more prolonged compared to that of **1** and **2**, and equilibrium is reached after several days with 45% of **3** to be hydrolyzed (Supporting Information, Figure S12). During the observation times, no release of the quinolone ligand from complexes **1**−**3** was detected. On the other hand, compound **4** has different behavior in aqueous solution: dmso release was observed within about the first 2 h, while after 2 weeks the release of the cin ligand was detected by the growth of a new set of resonances attributed to the free ligand. At equilibrium the ratio between **4**, **4a**, and free cinH was 13.8: 5.2: 1 (Supporting Information, Figure S13).

In general, compared to the neutral organometallic [Ru(η^6-p-cym)Cl(quinolonato)] complexes previously studied by us,[9,18,19] compounds **1**−**4** open up a coordination position more slowly and, above all, not quantitatively. In addition, contrary to what was observed for the organometallic quinolonato complexes, in the new coordination compounds, with exception of **4**, quinolones remained tightly bound to the metal center in aqueous solution even after a prolonged time, only in the case of **4** do we observe a partial release of the quinolone.

2.3. Bioassays. *2.3.1. DNA-Binding Studies.* Studies of the interaction of quinolones and their complexes with DNA are of great importance since their activity as antibacterial drugs presumably depends on the inhibition of DNA replication by targeting essential type II bacterial topoisomerases such as DNA gyrase and topoisomerase IV.[15] DNA can provide three distinct binding modes for quinolone metal complexes: binding to the groove, electrostatic binding to phosphate groups, and intercalation.

The changes observed in the UV spectra upon titration may provide evidence of the existing interaction mode, since a hypochromism due to $\pi \rightarrow \pi^*$ stacking interactions may appear in the case of the intercalative binding mode, while red-shift (bathochromism) may be observed when the DNA duplex is stabilized.[28]

The UV spectra have been recorded for a constant CT DNA concentration at different [complex]:[DNA] mixing ratios (r). The UV spectra of CT DNA in the presence of **1** at diverse r values (up to 0.3) are shown as examples in Figure 8A. Similar spectral changes were obtained when CT DNA was treated with complexes **2**−**4**, cinH and nalNa. The decrease of the intensity at λ_{max} = 258 nm is accompanied by a red-shift of the λ_{max} up to 265 nm for all compounds, suggesting that the interaction with CT DNA results in the direct formation of a new adduct with double-helical CT DNA.[29] The observed hypochromism may be attributed to stacking interaction between the aromatic chromophore of the compound and DNA base pairs consistent with the intercalative binding mode, while the red-shift is an evidence of the stabilization of the CT DNA duplex.[17,30]

The changes in the UV spectrum of a 2×10^{-5} M solution of the quinolones and complexes **1**−**4** during the titration upon addition of CT DNA in diverse r values may be observed in Figure 8 and Supporting Information, Figure S14. In the UV region, the intense absorption bands observed in the spectra of the complexes are attributed to the intraligand transition of the coordinated groups of quinolone ligands and could be perturbed in the case of interaction with CT DNA.[17,30]

In the UV spectrum of 2×10^{-5} M DMSO solution of cinH, the initial band at 357 nm displays a slight hypochromism upon addition of increasing amounts of CT DNA (up to $1/r = 2$). An additional band of increasing intensity appears at 375 nm, suggesting formation of a new adduct, which is also supported by the existence of a distinct isosbestic point at 367 nm (Figure 8B). In the UV spectrum of nalNa, the initial two bands at 333 and 345 nm (as a shoulder), respectively, present a hyperchromism upon addition of increasing amounts of CT DNA

dx.doi.org/10.1021/ic401220x | *Inorg. Chem.* XXXX, XXX, XXX−XXX

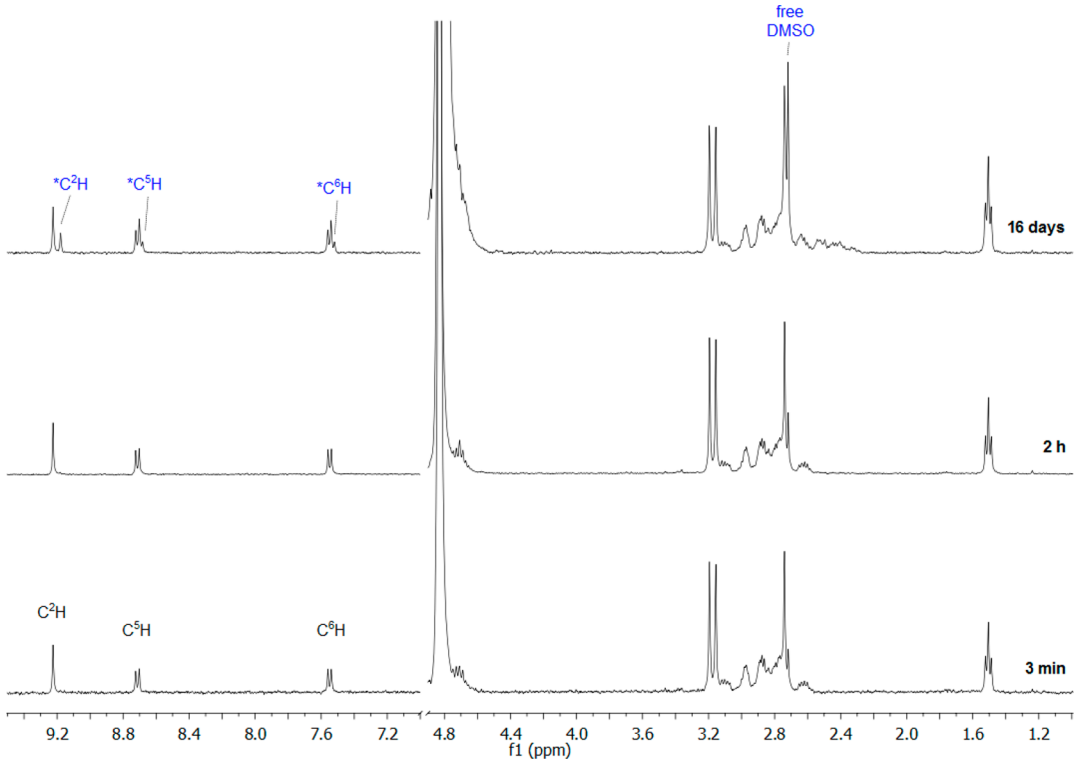

Figure 7. Time evolution ^{1}H NMR spectra of complex **2** (ca. 2.0 mM) in D_2O at room temperature. Selected resonances of the aqua species **2a** are indicated with an asterisk (*).

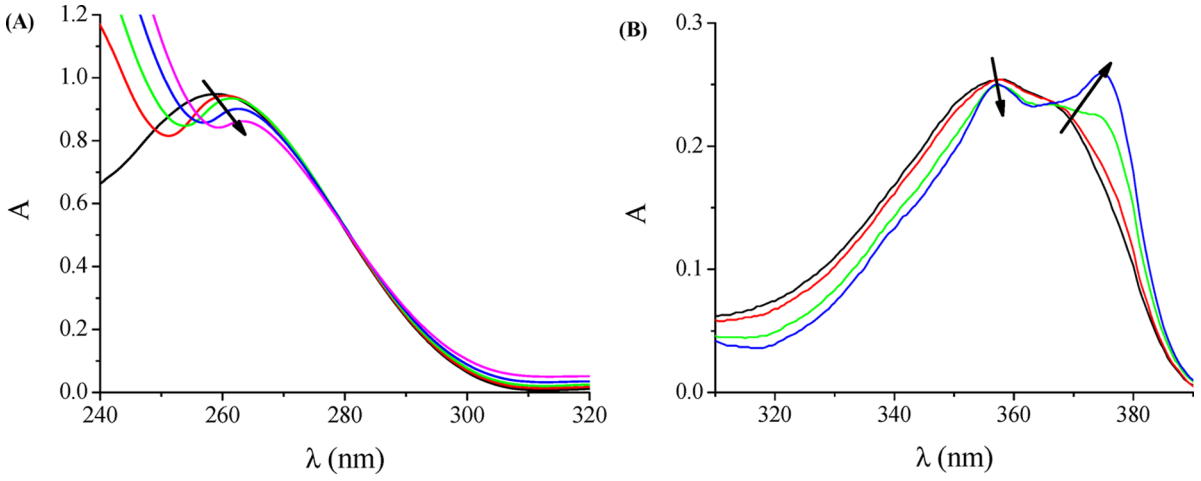

Figure 8. (A) UV spectra of CT DNA (1.44×10^{-4} M) in buffer solution (150 mM NaCl and 15 mM trisodium citrate at pH 7.0) in the absence or presence of **1**. The arrow shows the changes upon increasing amounts of complex (up to $r = 0.3$). (B) UV spectra of cinH (2×10^{-5} M) in DMSO solution in the presence of CT DNA at increasing amounts (up to $1/r = 2$). The arrows show the changes upon increasing amounts of CT DNA.

(up to $1/r = 2$) accompanied by a red-shift of 3 and 2 nm (to 336 and 347 nm), respectively (Supporting Information, Figure S15(A)). The observed spectral phenomena may suggest binding to CT DNA and stabilization.

In the UV spectrum of **1**, the band at 317 nm exhibits a slight hyperchromism while the absorbance of the band at 355 nm decreases slightly upon addition of CT DNA (Supporting Information, Figure S15(B)). In the UV spectrum of **2**, the band at 360 nm exhibits a slight hypochromism upon addition of CT DNA (Supporting Information, Figure S15(C)). In the UV spectrum of **3**, the band at 344 nm exhibits a slight hyperchromism upon addition of CT DNA followed by a blue-shift of 2 nm (to 342 nm) while the absorbance of a second band at 352 nm initially decreases and is followed by a slight increase of the absorbance accompanied by a 2 nm red-shift (to 354 nm) (Supporting Information, Figure S15(D)). In the UV spectrum of **4**, the band at 325 nm attributed to the intraligand transition in the quinolone ligand presents slight hyperchromism which is also observed for the band at 378 nm (Supporting Information, Figure S15(E)).

The results derived from the UV titration experiments suggest that all complexes can bind to CT DNA, although the exact mode of binding cannot be reliably proposed on the basis of UV spectroscopic titration studies.[17,30] The spectral behavior of the complexes upon addition of CT DNA suggests binding to CT DNA and stabilization while the existing differences may

dx.doi.org/10.1021/ic401220x | *Inorg. Chem.* XXXX, XXX, XXX−XXX

Table 2. DNA-Binding Constants (K_b) and Stern−Volmer Constants (K_{SV}) of the EB-DNA Quenching for the Quinolones and Complexes 1−4

compound	K_b (M^{-1})	K_{sv}
[Ru([9]aneS$_3$)(dmso-κS)(levo)](PF$_6$), **1**	2.02(±0.20) × 10^4	3.58(±0.22) × 10^5
[Ru([9]aneS$_3$)(dmso-κS)(nal)](PF$_6$), **2**	1.23(±0.30) × 10^4	7.57(±0.39) × 10^5
[Ru([9]aneS$_3$)(dmso-κS)(oxol)](PF$_6$), **3**	0.78(±0.03) × 10^4	1.83(±0.07) × 10^5
[Ru([9]aneS$_3$)(dmso-κS)(cin)](PF$_6$), **4**	1.55(±0.12) × 10^4	4.47(±0.25) × 10^5
levofloxacin. **levoH**[17]	4.36(±0.11) × 10^4	11.10(±0.30) × 10^5
sodium nalidixicate, **nalNa**	1.33(±0.12) × 10^4	3.53(±0.08) × 10^5
oxolinic acid, **oxolH**[32]	0.30(±0.01) × 10^4	
cinoxacin, **cinH**	1.26(±0.30) × 10^4	4.99(±0.21) × 10^5

Table 3. Cathodic and Anodic Potentials (in mV) for the Redox Couples (1) Ru(II)/Ru(I) and (2) Ru(II)/Ru(III) in DMSO Solution of the Complexes

complex	E_{pc}[a]	E_{pa}[a]	E_{pa}[b]	E_{pc}[b]	$E_{pc1'}$[c]	$E_{pa1'}$[c]	$E_{pa2'}$[c]
[Ru([9]aneS$_3$)(dmso-κS)(levo)](PF$_6$), **1**	−905	−745	−490	−492	−1050	−535	−360
[Ru([9]aneS$_3$)(dmso-κS)(nal)](PF$_6$), **2**	−885(lc)[d]	−705	−540(lc)[d]	−512	−1095	−920	−374
[Ru([9]aneS$_3$)(dmso-κS)(oxol)](PF$_6$), **3**	−835	−710	−460	−505	−1155	−590	−375
[Ru([9]aneS$_3$)(dmso-κS)(cin)](PF$_6$), **4**	−1360	−1275	−615	−505	−1335	−850	−375

[a] $E_{pc/a}$ of the redox couple Ru(II)/Ru(I). [b] $E_{pc/a}$ of the redox couple Ru(II)/Ru(III). [c] $E_{pc/a\ 1/2'}$ potentials that appear in second scan. [d] lc = low current.

Table 4. Cathodic and Anodic Potentials (in mV) for the Redox Couple Ru(II)/Ru(I) in 1:2 DMSO:Buffer Solution of the Complexes in the Absence and Presence of CT DNA

complex	$E_{pc(f)}$[a]	$E_{pc(b)}$[b]	ΔE_{pc}[c]	$E_{pa(f)}$[a]	$E_{pa(b)}$[b]	ΔE_{pa}[c]
[Ru([9]aneS$_3$)(dmso-κS)(levo)](PF$_6$), **1**	−705	−695	+10	−550	−550	0
[Ru([9]aneS$_3$)(dmso-κS)(nal)](PF$_6$), **2**	−703	−688	+15	−554	−554	0
[Ru([9]aneS$_3$)(dmso-κS)(oxol)](PF$_6$), **3**	−692	−685	+7	−565	−555	+10
[Ru([9]aneS$_3$)(dmso-κS)(cin)](PF$_6$), **4**	−697	−680	+17	−550	−557	−7

[a] $E_{pc/a(f)}$ in the absence of CT DNA. [b] $E_{pc/a(b)}$ in the presence of CT DNA. [c] $\Delta E_{pc/a} = E_{pc/a(b)} - E_{pc/a(f)}$.

be attributed to the quinolones. The existence of hypochromism and bathochromism in the spectra of CT DNA upon addition of **1**−**4** may be considered as first evidence that their binding via intercalation of the aromatic ligand accompanied by stabilization of the CT DNA duplex cannot be ruled out.[28]

The DNA-binding constant values, K_b, (Table 2) as calculated by Supporting Information, eq S1 and plots in Supporting Information, Figure S16 suggest a moderate binding of complexes **1**−**4** to CT DNA.[17,30] Comparison of the K_b values of complexes **1**−**4** with the corresponding quinolones (Table 2) shows that the values are of the same magnitude, with complex **1** exhibiting the highest K_b value among the complexes (2.02(±0.20)·× 10^4 M^{-1}). The K_b values of the complexes are of the same order of magnitude as the previously reported Ni(II) and Zn(II) complexes with oxolinato and levofloxacinato ligands.[17,30] However, they are lower than that of the classical intercalator EB, whose binding affinity for CT DNA is given by K_b = 1.23(±0.07)·10^5 M^{-1}.[17,30,31]

The cyclic voltammograms of **1** in DMSO solution (Supporting Information, Figure S17) exhibit a cathodic wave at −905 mV (E_{pc1}) followed by two anodic waves at −500 mV (E_{pa1}) and −320 mV (E_{pa2}), while in the second scan a new second cathodic wave appears at −490 mV (E_{pc2}) and the initial potentials $E_{pc1'}$, $E_{pa1'}$ and $E_{pa2'}$ shift to −1050, −535, and −360 mV, respectively. The wave with potentials E_{pc1} and E_{pa1} constitutes an irreversible redox process attributed to the Ru(II)/Ru(I) redox couple, while E_{pa2} and E_{pc2} exhibit much higher current intensity and can be attributed to a quasi-reversible Ru(II)/Ru(III) redox couple,[33] since the quinolones are electrochemically inactive. Complexes **2**−**4** exhibit similar electrochemical behavior in DMSO and the corresponding potentials are given in Table 3. In few cases, the current of the oxidation Ru(I) → Ru(II) is low and cannot be clearly detected.

In the cyclic voltammograms of the complexes in 0.4 mM 1:2 DMSO:buffer solution, only the potentials ($E_{pc(f)}$ and $E_{pa(f)}$, for the free complex) for the quasi-reversible redox couple Ru(II)/Ru(I) have been determined, and their values are given in Table 4. The changes of this redox couple Ru(II)/Ru(I) (up to r = 0.15) (Supporting Information, Figure S18) have been studied upon the addition of CT DNA (Supporting Information, Figure S17) and the potentials ($E_{pc(b)}$ and $E_{pa(b)}$, for the complex bound to CT DNA) as well as the corresponding shifts (ΔE_{pc} and ΔE_{pa}) are given in Table 4.

In general, the electrochemical potential of a small molecule shifts positively when it intercalates into the DNA double helix, whereas it will shift to a negative direction in the case of electrostatic interaction with DNA. Furthermore, when two or more potentials exist, a positive shift of E_{p1} and a negative shift of E_{p2} may imply that the molecule can bind to DNA by both intercalation and electrostatic interaction.[34] No new redox peaks appeared after the addition of CT DNA to each complex, while the current of all peaks decreased significantly suggesting the existence of an interaction between each complex and CT DNA. The decrease in current can be explained in terms of an equilibrium mixture of free and DNA-bound complex on the electrode surface. For increasing amounts of CT DNA (up to r = 0.15), at least one of the cathodic (E_{pc}) or the anodic (E_{pa}) potentials of complexes showed a positive shift (ΔE_{pc} = (+7)−(+17) mV) (Table 4) suggesting the existence of an

dx.doi.org/10.1021/ic401220x | Inorg. Chem. XXXX, XXX, XXX−XXX

intercalative binding mode, while for **4** the second potential shifted slightly to more negative values and the coexistence of electrostatic interaction cannot be ruled out.[17,30,32,35,36]

DNA viscosity is sensitive to DNA length change; therefore, its measurement upon addition of a compound provides a reliable evidence for the binding mode to DNA.[25,37] The addition of increasing amounts (up to r = 0.25) of complexes **1**–**4** to a DNA solution (0.1 mM) results in an increase in the relative viscosity of DNA (Figure 9), which is much more

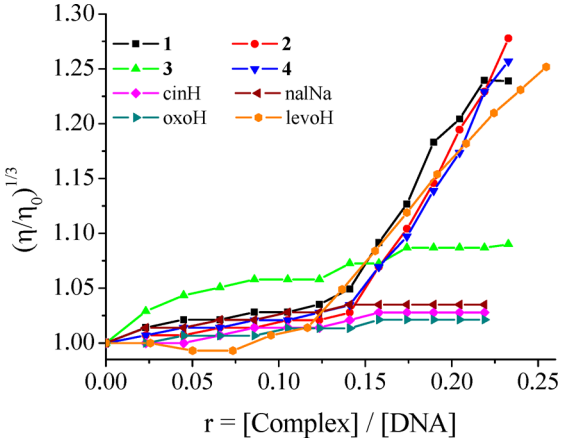

Figure 9. Relative viscosity $(\eta/\eta_o)^{1/3}$ of CT DNA (0.1 mM) in buffer solution (150 mM NaCl and 15 mM trisodium citrate at pH 7.0) in the presence of the quinolones or complexes **1**–**4** at increasing amounts (r).

pronounced upon addition of complexes **1**, **2**, and **4**. In the case of classic intercalation, DNA base pairs are separated to host the bound compound resulting in increased DNA viscosity, the magnitude of which is usually in accordance to the strength of the interaction, because of the lengthening of the DNA helix. Upon binding by means of partial and/or nonclassic intercalation in DNA grooves, the DNA solution viscosity is decreased or remains unchanged, since the DNA helix bend or kink may reduce slightly its effective length.[37] Therefore, the observed viscosity increase may be explained by an increase in overall DNA length provoked by the insertion of the compounds in between the DNA base pairs due to interaction via intercalation through the aromatic chromophore of quinolone ligands in the complexes.[30,32,35]

2.3.1.1. Competitive Studies with Ethidium Bromide. Ethidium bromide (EB = 3,8-diamino-5-ethyl-6-phenyl-phenanthridinium bromide) is a typical indicator of intercalation since it forms soluble complexes with nucleic acids and emits intense fluorescence in the presence of DNA because of the intercalation of the planar phenanthridine ring between the adjacent base pairs on the DNA double helix. Compounds **1**–**4** do not show any significant fluorescence at room temperature in solution or in the presence of CT DNA, when excited at 540 nm. Furthermore, the addition of complexes **1**–**4** to a solution containing EB does not provoke quenching of free EB fluorescence, and no new peaks appear in the spectra. The changes observed in the spectra of EB on its binding to CT DNA are often used for studying the interaction between DNA and other compounds, such as metal complexes, since the addition of a compound, capable of intercalating DNA equally or more strongly than EB, could result in a quenching of the EB-DNA fluorescence emission. The displacement of EB and/or electron transfer are the two mechanisms proposed to account for the decrease of the emission intensity.[38]

The emission spectra of EB bound to CT DNA in the absence and presence of each compound have been recorded for [EB] = 20 μM, [DNA] = 26 μM for increasing amounts of each compound up to the value of r = 0.08. The addition of each the quinolones or complexes **1**–**4** at diverse r values results in significant decrease of the intensity of the emission band (Figure 10) of the EB-DNA system at 592 nm indicating

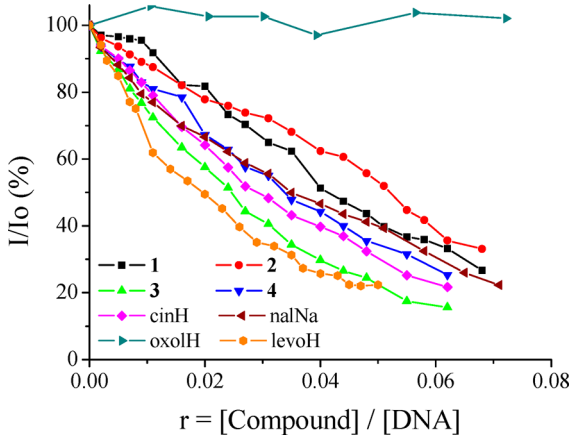

Figure 10. Plot of EB relative fluorescence intensity at λ_{em} = 592 nm (%) vs r (r = [Compound]/[DNA]) for complexes **1**–**4** and the quinolones (27% of the initial fluorescence intensity for **1**, 16% for **2**, 33% for **3**, 25% for **4**, 22% for cinH, 26% for nalNa, 100% for oxolH, and 23% for levoH) in buffer solution (150 mM NaCl and 15 mM trisodium citrate at pH 7.0).

the competition of the compounds with EB in binding to DNA. The observed quenching of EB-DNA fluorescence for the compounds suggests that they can displace EB from the EB-DNA complex and that they can probably interact with CT DNA by the intercalative mode.[30,32,35]

The Stern–Volmer plots of the EB-DNA quenching (Supporting Information, Figure S19) illustrate that the quenching provoked by the compounds is in good agreement (R = 0.99) with the linear Stern–Volmer equation (Supporting Information, eq S2) The Stern–Volmer constants values, K_{SV}, of the compounds are moderate to high (Table 2) showing that they can displace EB and bind relatively tightly to DNA.[30,32,35,39]

In general, the quenching of the EB-DNA fluorescence provoked by the complexes is similar to the queching provoked by the Zn(II)-quinolone complexes and more pronounced than by the Ni(II)-quinolone complexes reported.[17,30,32,39] The K_{SV} values of the Ru(II)-quinolone complexes are of the same order as the Zn(II)- and Ni(II)-quinolone complexes reported, although a direct correlation cannot be performed because of different coligands and metal environment.[39]

2.3.2. Albumin Binding Studies. The serum albumins (SAs) are the most abundant proteins in the circulation system and play important roles in the delivery of many pharmaceuticals to the sites of disease.[40] It is therefore important to study the interactions of biologically active compounds with these transport proteins since binding to these proteins may lead to loss or enhancement of the biological properties of the original drug, or provide paths for drug transportation. Interactions of metallodrugs with proteins are crucial for their biodistribution, toxicity, and even for their mechanism of action. For one of the

dx.doi.org/10.1021/ic401220x | Inorg. Chem. XXXX, XXX, XXX–XXX

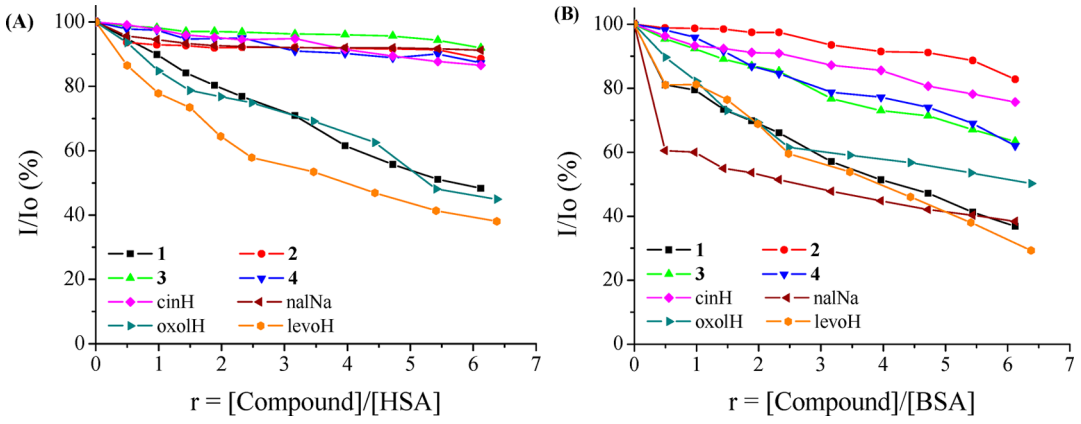

Figure 11. Plot of % relative fluorescence intensity at (A) λ_{em} = 351 nm (%) vs r (r = [complex]/[HSA]) for the quinolones and complexes **1**–**4** (48% of the initial fluorescence intensity for **1**, 88% for **2**, 92% for **3**, 87% for **4**, 87% for cinH, 91% for nalNa, 45% for oxolH, and 38% for levoH) and (B) λ_{em} = 342 nm (%) vs r (r = [complex]/[BSA]) for the quinolones and complexes **1**–**4** (37% of the initial fluorescence intensity for **1**, 83% for **2**, 63% for **3**, 62% for **4**, 75% for cinH, 38% for nalNa, 50% for oxolH, and 30% for levoH) in buffer solution (150 mM NaCl and 15 mM trisodium citrate at pH 7.0).

Table 5. SA Constants and Parameters (K_{sv}, k_q, K, n) Derived for Complexes 1–4 and the Free Quinolones

compound	K_{SV} (M^{-1})	k_q ($M^{-1}s^{-1}$)	K (M^{-1})	n
	BSA			
[Ru([9]aneS$_3$)(dmso-κS)(levo)](PF$_6$), **1**	8.89(±0.39) × 10^4	8.89(±0.39) × 10^{12}	8.59 × 10^4	0.99
[Ru([9]aneS$_3$)(dmso-κS)(nal)](PF$_6$), **2**	0.82(±0.01) × 10^4	0.82(±0.01) × 10^{12}	1.50 × 10^4	0.51
[Ru([9]aneS$_3$)(dmso-κS)(oxol)](PF$_6$), **3**	3.09(±0.10) × 10^4	3.09(±0.10) × 10^{12}	2.04 × 10^4	1.34
[Ru([9]aneS$_3$)(dmso-κS)(cin)](PF$_6$), **4**	3.07(±0.28) × 10^4	3.07(±0.28) × 10^{12}	3.77 × 10^4	0.74
levofloxacin. **levoH**[17]	9.47(±0.59) × 10^4	9.47(±0.59) × 10^{12}	3.59 × 10^4	1.71
sodium nalidixicate, **nalNa**	7.31(±0.09) × 10^4	7.31(±0.09) × 10^{12}	31.0 × 10^4	0.71
oxolinic acid, **oxolH**[32]	5.01(±0.22) × 10^4	5.01(±0.22) × 10^{12}	10.9 × 10^4	0.75
cinoxacin, **cinH**	1.70(±0.09) × 10^4	1.70(±0.09) × 10^{12}	1.57 × 10^4	1.07
	HSA			
[Ru([9]aneS$_3$)(dmso-κS)(levo)](PF$_6$), **1**	5.98(±0.25) × 10^4	5.98(±0.25) × 10^{12}	2.01 × 10^4	0.92
[Ru([9]aneS$_3$)(dmso-κS)(nal)](PF$_6$), **2**	0.15(±0.02) × 10^4	0.15(±0.02) × 10^{12}	43.6 × 10^4	0.10
[Ru([9]aneS$_3$)(dmso-κS)(oxol)](PF$_6$), **3**	0.31(±0.03) × 10^4	0.31(±0.03) × 10^{12}	12.4 × 10^4	0.07
[Ru([9]aneS$_3$)(dmso-κS)(cin)](PF$_6$), **4**	0.80(±0.03) × 10^4	0.80(±0.03) × 10^{12}	7.59 × 10^4	0.21
levofloxacin. **levoH**[17]	0.84(±0.02) × 10^4	0.84(±0.02) × 10^{12}	11.5 × 10^4	0.89
sodium nalidixicate, **nalNa**	0.22(±0.03) × 10^4	0.22(±0.03) × 10^{12}	58.1 × 10^4	0.09
oxolinic acid, **oxolH**[32]	6.39(±0.26) × 10^4	6.39(±0.26) × 10^{12}	11.3 × 10^4	0.60
cinoxacin, **cinH**	0.84(±0.02) × 10^4	0.84(±0.02) × 10^{12}	0.47 × 10^4	0.85

most representative ruthenium anticancer drug candidates, KP1019, it was found that rapid binding occurs in a noncovalent manner at the hydrophobic binding sites of HSA, but longer exposure results in a protein-coordinated form.[41] We have previously studied the interactions between HSA and the organoruthenium-quinolone complexes by means of ICP-MS coupled with capillary zone electrophoresis and have found that protein binding occurs rapidly with more than 90% of the ruthenium being bound within 20 min.[19] Since complexes **1**–**4** have shown notable differences in their physicochemical properties compared to their organometallic counterparts, the main difference being the kinetic inertness to ligand substitution in aqueous solution, we were interested to see if the complexes still show the affinity toward proteins. In this study, the interaction between BSA/HSA (bovine/human serum albumin) and the ruthenium-quinolone complexes was investigated by fluorescence spectroscopy as this method allows a quantitative assessment of the binding strength.

BSA is the most extensively studied serum albumin because of its high structural homology with HSA. BSA has two tryptophan residues, Trp-134 and Trp-212, whereas HSA has a single tryptophan located at position 214. Both BSA and HSA can bind reversibly to a large number of compounds.[42] BSA and HSA solutions exhibit an intense fluorescence emission with a peak at 342 and 351 nm, respectively, due to the tryptophan residues, when excited at 295 nm.[26] The changes and the quenching observed in the fluorescence emission spectra of tryptophan in BSA or HSA upon addition of complexes **1**–**4** are primarily due to changes in protein conformation, subunit association, substrate binding, or denaturation.

Addition of the quinolones or complexes **1**–**4** to a SA solution (up to r values of 7) results in a moderate quenching of the HSA fluorescence at λ = 351 nm for **1**, oxolH and levoH and lower quenching for complexes **2**–**4**, cinH and nalNa (Figure 11A) while in the case of BSA the quenching of the fluorescence at λ = 342 nm is more significant (Figure 11B). The observed quenching may be attributed to changes in protein tertiary structure leading to changes in tryptophan environment of SA, and thus indicating the binding of each compound to the albumins.[42]

The calculated values of Stern–Volmer quenching constant (K_{sv}) and quenching rate constant (k_q) for the interaction of

dx.doi.org/10.1021/ic401220x | Inorg. Chem. XXXX, XXX, XXX–XXX

the compounds with the SAs (from Supporting Information, eqs S3 and S4 and Figures S20 and S21) are given in Table 5 and indicate relatively good quenching ability of the SA fluorescence, with **1** exhibiting the highest k_q value for both albumins. Furthermore, the k_q values ($>10^{11}$ M^{-1} s^{-1}) are higher than diverse kinds of quenchers for biopolymer fluorescence (2.0×10^{10} M^{-1} s^{-1}) indicating the existence of a static quenching mechanism.[42]

The values of the SA-binding constant (K) and the number of binding sites per albumin (n), as calculated from the Scatchard equation (Supporting Information, eq S5)[43] and Scatchard plots (Supporting Information, Figures S22 and S23) for the compounds are given in Table 5. The highest binding constant to BSA (K) is found for complex **1** and to HSA for complex **2**. Additionally, complexes **3** and **1** present the highest number of binding sites per albumin (n) among the complexes for BSA and HSA, respectively. Comparing the affinity of complexes **1**−**4** for BSA and HSA (K values), it is obvious (Table 5) that complexes **2**−**4** show higher affinity for HSA than BSA, while **1** exhibits higher binding constant for BSA than for HSA.

The values of the quenching rate constant (k_q) and the SA binding constant (K) found for complexes **1**−**4** are similar to the values reported for a series of zinc and nickel complexes bearing oxolinato and levofloxacinato ligand, although a more detailed comparison cannot be performed since the coligands are different (N-donor ligands).[17,30,32,39] The SA-binding constants (K) of all compounds studied are within the range which could be considered optimal; they are high enough so that the compounds bind to SA to get transport, but nevertheless they are sufficiently low (i.e., below the value of 10^{15} M^{-1}, which is the association constant of avidin with diverse ligands; this interaction is considered the strongest among known noncovalent interactions) so that the compounds can be released from the albumin upon arrival at the target cells.[39,43]

2.3.3. Cathepsin Inhibition and Cytotoxicity of the Compounds. Having found that the complexes **1**−**4** can bind to serum proteins and DNA, we were interested to evaluate whether they can bind to enzymes involved in cancer progression. Among these are also proteases from the cysteine cathepsin family, which are known to have a major role in various stages of cancer progression, as demonstrated by inhibition studies and gene ablation studies in animal cancer models.[44] Moreover, they are known to bind to various metal complexes because of their free cysteine in the active site.[10,45] The studies were focused on cathepsins B and S, which are among the cathepsins most often linked with cancer progression. Compounds **2** and **4** exhibited weak inhibition of the two cathepsins, whereas compounds **1** and **3** were inactive (Table 6). These interactions are substantially weaker than that observed earlier for the organoruthenium complex with 4-thionalidixic acid but may not be relevant for the in vivo studies, suggesting that organoruthenium complexes may have other/additional, perhaps more important targets in vivo.[9]

In vitro cytotoxicity assays were performed on human cervix carcinoma (HeLa) and non small cell lung carcinoma (A549) cells. All four tested ruthenium compounds exhibited modest activity against HeLa cell line. However, only the precursor **P1** showed moderate activity against the A549 cell line, whereas compounds **1**, **2**, and **4** exhibited only a very low cytotoxic activity over the concentration range used and only an estimate (IC_{50} > 600 μM) could be given (Table 7). These results are similar to those of the organoruthenium complexes tested before.[9] However, all these cell lines are derived from primary tumors and may not be the best models for metastasis spread, where ruthenium complexes were found to be the most efficient in vivo. This has been clearly shown for the compound NAMI-A, which is not cytotoxic in vitro but highly active against metastases in vivo. Therefore, the high IC_{50} values alone are not a sufficient reason to discard a compound as a potential drug candidate.[3,46] It can be suggested that further in vivo studies would be needed to evaluate whether these compounds exhibit antitumor/antimetastatic effect.

Table 6. IC_{50} (μM) Values for Inhibition of Human Cathepsins B and S by Compounds 1−4 at pH 6.0[a]

	cathepsin B	cathepsin S
1	540 ± 57	>500
2	377 ± 22	200 ± 22
3	>500	>500
4	236 ± 23	318 ± 10

[a]All experimental conditions were as described in the Materials and Methods section. IC_{50} values are given together with their standard errors.

Table 7. IC_{50} (μM) Values for the Cytotoxicity of the Compounds 1, 2, 4, and P1 on HeLa and A549 Human Tumor Cell Lines[a]

	HeLa	A549
1	227 ± 40	>600
2	475 ± 115	>600
4	394 ± 98	>600
P1	440 ± 94	454 ± 44

[a]All experimental conditions were as described in the Materials and Methods section. IC_{50} values are given together with their standard errors.

3. CONCLUSION

A study of the stability and behavior in aqueous solution of novel metal compounds with potential anticancer activity is essential for further studies of interactions with potential targets including DNA, serum proteins, and enzymes. In our previous work we have reported the synthesis and physicochemical characterization of four neutral organoruthenium compounds with quinolones of the general formula [Ru(η^6-cymene)(quinolonato-κ^2O,O)Cl], and we have thoroughly investigated their stability and behavior in aqueous solution.[9,18,19] The organometallic compounds undergo a fast release of the chlorido ligand forming the corresponding [Ru(η^6-cymene)(*O*,*O*′-quinolonato)(OH_2)]$^+$ species which, in turn, slowly release the quinolone ligand, reaching an equilibrium after about 24 h in which 10−50% of the quinolone is free. The trithiacyclononane complexes of the general formula [Ru([9]-aneS_3)(dmso-κS)(quinolonato-κ^2O,O)](PF_6) reported herein have much higher stability since the release of the auxiliary ligand dmso is very slow compared to the chlorido ligand in the organometallic counterparts, and the quinolone is not released either. UV spectroscopy, viscosity measurements, and cyclic voltammetry studies have revealed the ability of the complexes to bind to CT DNA. The UV spectroscopic titrations have shown that complexes **1**−**4** exhibit similar K_b values with CT DNA. Competitive binding studies with EB have revealed the ability of the complexes to displace EB from the EB-DNA

dx.doi.org/10.1021/ic401220x | *Inorg. Chem.* XXXX, XXX, XXX−XXX

complex, and cyclic voltammetry titration studies as well as viscosity measurements have confirmed intercalation as the most probable binding mode to DNA. All complexes show good binding affinity to BSA and HSA, with relatively high binding constants. Compounds **2** and **4** also exhibit moderate inhibitory properties toward cathepsins B and S, two members of the cathepsin family involved in cancer development and progression. All four tested compounds exhibited modest cytotoxicity against one of the tested cancer cell lines (HeLa). This study provides additional confirmation that ruthenium complexes could indeed have multiple targets and mechanisms of action. Finding new uses for old drugs[47] and incorporation of a bioactive functionality into a structure that can operate in a synergistic way with the metal moiety[48] are two well established concepts in modern drug design. Our studies have clearly confirmed that quinolone antibacterial agents may be converted to ruthenium complexes that exert interesting physicochemical and biological properties. Moreover, our results also show that even minor changes in the structure of the quinolone ligands may substantially change the physicochemical and biological properties of their Ru complexes. This is the case of **3** and **4**, whose quinolone ligands differ only in one nitrogen atom, yet display significantly different aqueous solubility and hydrolytic behavior. Interestingly, these differences do not influence much the type and strength of the interactions with the biomolecules used in our study. At this stage it is still difficult to find a clear correlation between the structure and function data, and more work is needed for better understanding.

■ ASSOCIATED CONTENT

Ⓢ Supporting Information

Tables S1a and S1b as well as cif files giving crystallographic data for compounds **2** and **4**. Figures (S1−S23) and Tables (S2−S4) containing NMR, UV, and CV data for the compounds as well as the plots and equations (S1−S5) used for the quantitative assessment of the interactions with DNA, HSA, and BSA and fluorescence experiments. This material is available free of charge via the Internet at http://pubs.acs.org. The cif files were submitted to CCDC and have been allocated the deposition numbers CCDC 947546 and 947547 for **2** and **4**, respectively.

■ AUTHOR INFORMATION

Corresponding Author

*E-mail: iztok.turel@fkkt.uni-lj.si.

Notes

The authors declare no competing financial interest.

■ ACKNOWLEDGMENTS

We are grateful to the Slovenian Research Agency (ARRS) for the junior research grants for J.K. and M.B., the project grant J1-4131 (IT), and the program grant P1-0140 (BT). The project was supported by COST actions CM1105 and D39, in particular for a short term scientific mission of I.B. to Ljubljana.

■ REFERENCES

(1) Wong, E.; Giandomenico, C. M. *Chem. Rev.* **1999**, *99*, 2451−2466.

(2) Alessio, E., Ed.; *Bioinorganic Medicinal Chemistry*; Wiley-VCH Verlag & Co. KGaA: Weinheim, Germany, 2011.

(3) Rademaker-Lakhai, J. M.; van den Bongard, D.; Pluim, D.; Beijnen, J. H.; Schellens, J. H. M. *Clin. Cancer Res.* **2004**, *10*, 3717−3727.

(4) Hartinger, C. G.; Jakupec, M. A.; Zorbas-Seifried, S.; Groessl, M.; Egger, A.; Berger, W.; Zorbas, H.; Dyson, P. J.; Keppler, B. K. *Chem. Biodiversity* **2008**, *5*, 2140−2155.

(5) (a) Yan, Y. K.; Melchart, M.; Habtemariam, A.; Sadler, P. J. *Chem. Commun.* **2005**, *38*, 4764−4776. (b) Dougan, S.; Sadler, P. J. *Chimia* **2007**, *61*, 704−715. (c) Renfrew, A. K.; Phillips, A. D.; Egger, A. E.; Hartinger, C. G.; Bosquain, S. S.; Nazarov, A. A.; Keppler, B. K.; Gonsalvi, L.; Peruzzini, M.; Dyson, P. J. *Organometallics* **2009**, *28*, 1165−1172. (d) Renfrew, A. K.; Phillips, A. D.; Tapavicza, E.; Scopelliti, R.; Rothlisberger, U.; Dyson, P. J. *Organometallics* **2009**, *28*, 5061−5071.

(6) (a) Serli, B.; Zangrando, E.; Gianferrara, T.; Scolaro, C.; Dyson, P. J.; Bergamo, A.; Alessio, E. *Eur. J. Inorg. Chem.* **2005**, *17*, 3423−3434. (b) Bratsos, I.; Jedner, S.; Bergamo, A.; Sava, G.; Gianferrara, T.; Zangrando, E.; Alessio, E. *J. Inorg. Biochem.* **2008**, *102*, 1120−1133. (c) Bratsos, I.; Urankar, D.; Zangrando, E.; Genova-Kalou, P.; Kosmrlj, J.; Alessio, E.; Turel, I. *Dalton Trans.* **2011**, *40*, 5188−5199.

(7) Bratsos, I.; Birarda, G.; Jedner, S.; Zangrando, E.; Alessio, E. *Dalton Trans.* **2007**, *36*, 4048−4058.

(8) (a) Ang, W. H.; De Luca, A.; Chapuis-Bernasconi, C.; Juillerat-Jeanneret, L.; Lo Bello, M.; Dyson, P. J. *ChemMedChem* **2007**, *2*, 1799−1806. (b) Ang, W. H.; Parker, L. J.; De Luca, A.; Juillerat-Jeanneret, L.; Morton, C. J.; Lo Bello, M.; Parker, M. W.; Dyson, P. J. *Angew. Chem., Int. Ed.* **2009**, *48*, 3854−3857.

(9) Hudej, R.; Kljun, J.; Kandioller, W.; Repnik, U.; Turk, B.; Hartinger, C. G.; Keppler, B. K.; Miklavcic, D.; Turel, I. *Organometallics* **2012**, *31*, 5867−5874.

(10) Casini, A.; Gabbiani, C.; Sorrentino, F.; Rigobello, M. P.; Bindoli, A.; Geldbach, T. J.; Marrone, A.; Re, N.; Hartinger, C. G.; Dyson, P. J.; Messori, L. *J. Med. Chem.* **2008**, *51*, 6773−6781.

(11) (a) Andriole, V. T. *The Quinolones*, 3rd ed.; Academic Press: San Diego, CA, 2000; (b) Hooper, D. C.; Rubinstein, E. *Quinolone Antimicrobial Agents*, 3rd ed.; ASM Press: Washington, DC, 2003; (c) Ronald, A. R.; Low, D. E. *Fluoroquinolone antibiotics*; Birkhäuser Verlag: Basel, Switzerland, 2003.

(12) Kwok, Y.; Zeng, Q. P.; Hurley, L. H. *J. Biol. Chem.* **1999**, *274* (24), 17226−17235.

(13) Mitscher, L. A. *Chem. Rev.* **2005**, *105*, 559−592.

(14) Wohlkonig, A.; Chan, P. F.; Fosberry, A. P.; Homes, P.; Huang, J. Z.; Kranz, M.; Leydon, V. R.; Miles, T. J.; Pearson, N. D.; Perera, R. L.; Shillings, A. J.; Gwynn, M. N.; Bax, B. D. *Nat. Struct. Mol. Biol.* **2010**, *17*, 1152−1153.

(15) Turel, I. *Coord. Chem. Rev.* **2002**, *232*, 27−47.

(16) (a) Katsarou, M. E.; Efthimiadou, E. K.; Psomas, G.; Karaliota, A.; Vourloumis, D. *J. Med. Chem.* **2008**, *51*, 470−478. (b) Drevensek, P.; Zupancic, T.; Pihlar, B.; Jerala, R.; Kolitsch, U.; Plaper, A.; Turel, I. *J. Inorg. Biochem.* **2005**, *99*, 432−442. (c) Turel, I.; Zivec, P.; Pevec, A.; Tempelaar, S.; Psomas, G. *Eur. J. Inorg. Chem.* **2008**, *23*, 3718−3727.

(17) Tarushi, A.; Polatoglou, E.; Kljun, J.; Turel, I.; Psomas, G.; Kessissoglou, D. P. *Dalton Trans.* **2011**, *40*, 9461−9473.

(18) Turel, I.; Kljun, J.; Perdih, F.; Morozova, E.; Bakulev, V.; Kasyanenko, N.; Byl, J. A. W.; Osheroff, N. *Inorg. Chem.* **2010**, *49*, 10750−10752.

(19) Kljun, J.; Bytzek, A. K.; Kandioller, W.; Bartel, C.; Jakupec, M. A.; Hartinger, C. G.; Keppler, B. K.; Turel, I. *Organometallics* **2011**, *30*, 2506−2512.

(20) Bratsos, I.; Mitri, E.; Ravalico, F.; Zangrando, E.; Gianferrara, T.; Bergamo, A.; Alessio, E. *Dalton Trans.* **2012**, *41*, 7358−7371.

(21) Otwinowski, Z.; Minor, Z. Processing of X-ray Diffraction Data Collected in Oscillation Mode. *Methods in Enzymology*; Carter, C.W., Jr., Sweet, R. M., Eds; Academic Press: New York, **1997**; Macromolecular Crystallography, Vol. *276* part A, pp 307−326.

(22) Altomare, A.; Cascarano, G.; Giacovazzo, C.; Guagliardi, A. C.; Burla, M. C.; Polidori, G.; Camalli, M. *J. Appl. Crystallogr.* **1994**, *27*, 435.

(23) Sheldrick, G. M. *Acta Crystallogr., Sect. A* **2008**, *64*, 112−122.

(24) (a) Macrae, C. F.; Edgington, P. R.; McCabe, P.; Pidcock, E.; Shields, G. P.; Taylor, R.; Towler, M.; van De Streek, J. *J. Appl.*

Crystallogr. **2006**, *39*, 453−457. (b) Spek, A. L. *Acta Crystallogr., Sect. D: Biol. Crystallogr.* **2009**, *65*, 148−155.
(25) Li, D. D.; Tian, J. L.; Gu, W.; Liu, X.; Yan, S. P. *J. Inorg. Biochem.* **2010**, *104*, 171−179.
(26) Lakowicz, J. R. *Principles of Fluorescence Spectroscopy*, 3rd ed.; Springer: New York, 2006.
(27) (a) Bromme, D.; Nallaseth, F. S.; Turk, B. *Methods* **2004**, *32*, 199−206. (b) Mihelic, M.; Dobersek, A.; Guncar, G.; Turk, D. *J. Biol. Chem.* **2008**, *283*, 14453−14460. (c) Rozman, J.; Stojan, J.; Kuhelj, R.; Turk, V.; Turk, B. *FEBS Lett.* **1999**, *459*, 358−362.
(28) Pyle, A. M.; Rehmann, J. P.; Meshoyrer, R.; Kumar, C. V.; Turro, N. J.; Barton, J. K. *J. Am. Chem. Soc.* **1989**, *111*, 3051−3058.
(29) Song, Y.; Wu, Q.; Yang, P.; Luan, N.; Wang, L.; Liu, Y. *J. Inorg. Biochem.* **2006**, *100*, 1685−1691.
(30) Tarushi, A.; Lafazanis, K.; Kljun, J.; Turel, I.; Pantazaki, A. A.; Psomas, G.; Kessissoglou, D. P. *J. Inorg. Biochem.* **2013**, *121*, 53−65.
(31) Dimitrakopoulou, A.; Dendrinou-Samara, C.; Pantazaki, A. A.; Alexiou, M.; Nordlander, E.; Kessissoglou, D. P. *J. Inorg. Biochem.* **2008**, *102*, 618−628.
(32) Tarushi, A.; Psomas, G.; Raptopoulou, C. P.; Kessissoglou, D. P. *J. Inorg. Biochem.* **2009**, *103*, 898−905.
(33) (a) Sumiyoshi, T.; Gunnoe, T. B.; Petersen, J. L.; Boyle, P. D. *Inorg. Chim. Acta* **2008**, *361*, 3254−3262. (b) Kennedy, D. C.; Wu, A.; Patrick, B. O.; James, B. R. *J. Inorg. Biochem.* **2006**, *100*, 1974−1982.
(34) (a) Carter, M. T.; Rodriguez, M.; Bard, A. J. *J. Am. Chem. Soc.* **1989**, *111*, 8901−8911. (b) Jiao, K.; Wang, Q.; Sun, W.; Jian, F. *J. Inorg. Biochem.* **2005**, *99*, 1369−1375.
(35) Koumousi, E. S.; Zampakou, M.; Raptopoulou, C. P.; Psycharis, V.; Beavers, C. M.; Teat, S. J.; Psomas, G.; Stamatatos, T. C. *Inorg. Chem.* **2012**, *51*, 7699−7710.
(36) Skyrianou, K. C.; Perdih, F.; Papadopoulos, A. N.; Turel, I.; Kessissoglou, D. P.; Psomas, G. *J. Inorg. Biochem.* **2011**, *105*, 1273−1285.
(37) Jiang, M.; Li, Y.; Wu, Z.; Liu, Z.; Yan, C. *J. Inorg. Biochem.* **2009**, *103*, 833−844.
(38) (a) Zhao, G.; Lin, H.; Zhu, S.; Sun, H.; Chen, Y. *J. Inorg. Biochem.* **1998**, *70*, 219−226. (b) Pasternack, R. F.; Caccam, M.; Keogh, B.; Stephenson, T. A.; Williams, A. P.; Gibbs, F. J. *J. Am. Chem. Soc.* **1991**, 113.
(39) Psomas, G.; Kessissoglou, D. P. *Dalton Trans.* **2013**, *42*, 6252−6276.
(40) Timerbaev, A. R.; Hartinger, C. G.; Aleksenko, S. S.; Keppler, B. K. *Chem. Rev.* **2006**, *106*, 2224−2248.
(41) Dömötör, O.; Hartinger, C. G.; Bytzek, A. K.; Kiss, T.; Keppler, B. K.; Enyedy, E. A. *J. Biol. Inorg. Chem.* **2013**, *18*, 9−17.
(42) (a) Wang, Y.; Zhang, H.; Zhang, G.; Tao, W.; Tang, S. *J. Lumin.* **2007**, *126*, 211−218. (b) Deepa, S.; Mishra, A. K. *J. Pharm. Biomed. Anal.* **2005**, *38*, 556−563. (c) Lakowicz, J. R.; Weber, G. *Biochemistry* **1973**, *12*, 4161−4170.
(43) (a) Wu, S.; Yuan, W.; Wang, H.; Zhang, Q.; Liu, M.; Yu, K. *J. Inorg. Biochem.* **2008**, *102*, 2026−2034. (b) Rajendiran, V.; Karthik, R.; Palaniandavar, M.; Stoeckli-Evans, H.; Periasamy, V. S.; Akbarsha, M. A.; Srinag, B. S.; Krishnamurthy, H. *Inorg. Chem.* **2007**, *46*, 8208−8221.
(44) (a) Gocheva, V.; Zeng, W.; Ke, D. X.; Klimstra, D.; Reinheckel, T.; Peters, C.; Hanahan, D.; Joyce, J. A. *Genes Dev.* **2006**, *20*, 543−556. (b) Vasiljeva, O.; Korovin, M.; Gajda, M.; Brodoefel, H.; Bojic, L.; Kruger, A.; Schurigt, U.; Sevenich, L.; Turk, B.; Peters, C.; Reinheckel, T. *Oncogene* **2008**, *27*, 4191−4199.
(45) (a) Cunha, R. L. O. R.; Urano, M. E.; Chagas, J. R.; Almeida, P. C.; Bincoletto, C.; Tersariol, I. L. S.; Comasseto, J. V. *Bioorg. Med. Chem. Lett.* **2005**, *15*, 755−760. (b) Piovan, L.; Alves, M. F. M.; Juliano, L.; Bromme, D.; Cunha, R. L. O. R.; Andrade, L. H. *Bioorg. Med. Chem.* **2011**, *19*, 2009−2014. (c) Zhu, Y. B.; Cameron, B. R.; Mosi, R.; Anastassov, V.; Cox, J.; Qin, L.; Santucci, Z.; Metz, M.; Skerlj, R. T.; Fricker, S. P. *J. Inorg. Biochem.* **2011**, *105*, 754−762. (d) Fricker, S. P. *Metallomics* **2010**, *2*, 366−377. (e) Mosi, R.; Baird, I. R.; Cox, J.; Anastassov, V.; Cameron, B.; Skerlj, R. T.; Fricker, S. P. *J. Med. Chem.* **2006**, *49*, 5262−5272.
(46) Sava, G.; Capozzi, I.; Clerici, K.; Gagliardi, G.; Alessio, E.; Mestroni, G. *Clin. Exp. Metastasis* **1998**, *16*, 371−379.
(47) Chong, C. R.; Sullivan, D. J. *Nature* **2007**, *448*, 645−646.
(48) Hartinger, C. G.; Metzler-Nolte, N.; Dyson, P. J. *Organometallics* **2012**, *31*, 5677−5685.

dx.doi.org/10.1021/ic401220x | *Inorg. Chem.* XXXX, XXX, XXX−XXX